Stripping chronopotentiometry at scanned deposition potential (SSCP) : an effective methodology for dynamic speciation analysis of nanoparticulate metal complexes

Stripping chronopotentiometry at scanned deposition potential (SSCP): an effective methodology for dynamic speciation analysis of nanoparticulate metal complexes

Raewyn M. Town[a,b*] and Herman P. van Leeuwen[b]

[a] Systemic Physiological and Ecotoxicological Research (SPHERE), Department of Biology, Universiteit Antwerpen, Groenenborgerlaan 171, 2020 Antwerpen, Belgium. Corresponding author: raewyn.town@uantwerpen.be

[b] Physical Chemistry and Soft Matter, Wageningen University & Research, Stippeneng 4, 6708 WE Wageningen, The Netherlands

Highlights

- Depletive SCP quantitatively oxidises accumulated M^0 from the Hg electrode volume
- SSCP can unambiguously distinguish between various metal complex reactivity features
- Thermodynamic and kinetic descriptors are derived from SSCP waves
- SSCP facilitates characterisation of reactivity of nanoparticulate metal complexes

Abstract

The features of stripping chronopotentiometry at scanned deposition potential (SSCP) are reviewed and placed in context with voltammetric and other dynamic speciation techniques. The advantages of SSCP for speciation analysis of nanoparticulate metal complexes are highlighted. Analogous to other electrochemical techniques, the SSCP wave is rich in information: the measurements from the foot to the plateau of the wave access the relevant parts of the stability distribution and the rate constant distributions. The complete depletion regime of SSCP offers particular advantages due to its ability to unambiguously distinguish between various factors that can confound interpretation of data from other electroanalytical methods, including electrochemical irreversibility, kinetically controlled currents, reduced diffusion coefficient of the metal complex species as compared to the free metal ion, and chemical heterogeneity in the intrinsic binding affinity.

Grapical abstract

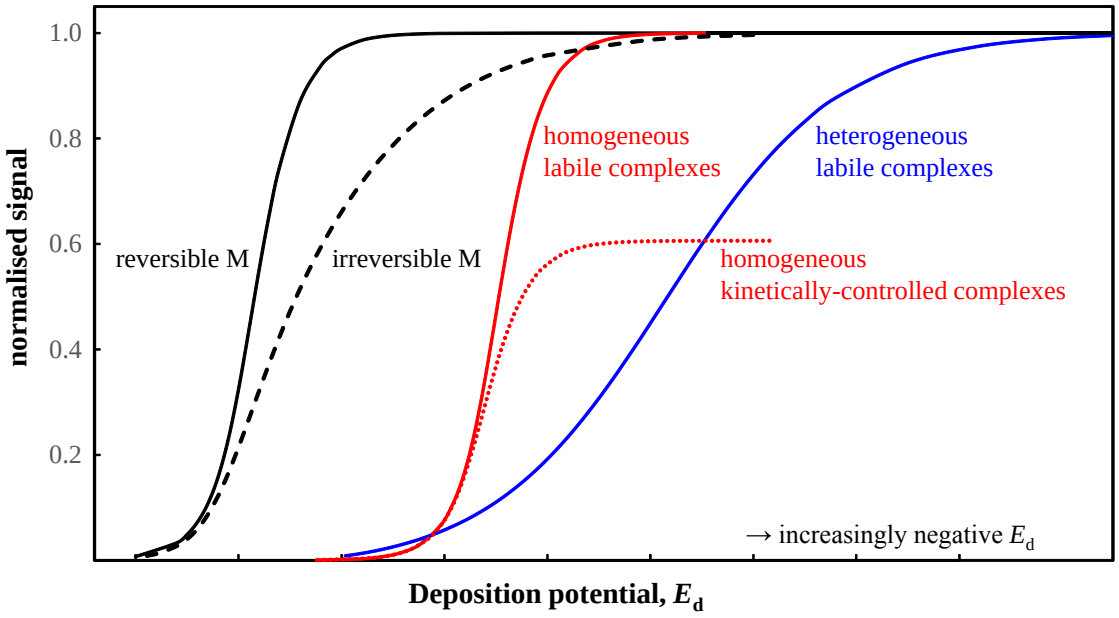

Keywords: dynamic metal speciation; nanoparticulate complexants; lability; chemical heterogeneity; humic substances

1. Introduction

Various electrochemical techniques are powerful tools for dynamic metal ion speciation analysis. They generally are inherently rich in information content, e.g. a voltammetric current vs potential curve or a chronopotentiometric potential time dependence scans the relevant part(s) of the stability distribution of the different complex species and the corresponding parts of the complex formation/dissociation rate constant distributions. Accordingly, electrochemical methods enable both the thermodynamic and kinetic descriptors of metal ion complexes to be determined [1-6]. Due to their low detection limits (bulk metal ion concentrations down to the order of nanomolar), electrochemical techniques which include a preconcentration step, e.g. various modes of stripping voltammetry (SV) and stripping chronopotentiometry (SCP), find wide application in metal speciation analysis of aquatic environmental systems [1-16]. Still, the interpretation of single stripping signals can be rather involved. Notably, when the accumulated metal is not completely removed from the electrode during the stripping step, the signal is prone to interference by secondary factors such as induced metal adsorption on the electrode surface [17-24], or saturation of ligand at the electrode surface during the stripping (re-oxidation) step [24-27]. Depletive stripping chronopotentiometry (SCP) overcomes these limitations [20,24,27]. In particular, depletive SCP at scanned deposition potential (SSCP) is established as a particularly powerful comprehensive approach for metal speciation analysis [28-30]. An SSCP curve is constructed by plotting the depletive SCP analytical signal (i.e. the reoxidation transition time, τ) as a function of the deposition potential, E_d (also often denoted as the accumulation potential). Analogous to conventional voltammograms, SSCP waves access the relevant parts of the stability distribution and the rate constant distributions. This situation is a major advantage over other

non-equilibrium speciation techniques which are typically configured for limiting steady-state flux conditions, e.g. diffusive gradients in thin film (DGT) [31,32], and the kinetic modes of the Donnan membrane technique (DMT) [33,34] and permeation liquid membranes (PLM) [35-37]. Whilst manipulation of the flux conditions at the reactive interface is in principle possible with DGT, DMT and PLM, e.g. by changing the affinity of the accumulating phase for the target species [38], this is less readily achieved and is not routine practice *cf*. the inherent nature of electrochemical methods in this regard. Speciation techniques each have their own effective timescale, governed by the pertaining characteristic diffusion length, which determines the range of metal complex species that are detectable [39]. The effective timescale of non-equilibrium speciation techniques can be varied by changing the electrode size (electrochemical methods [40-42]), changing the hydrodynamic conditions by manipulating the flow in the bulk medium (electrochemical methods, DGT, DMT, PLM) or by varying the thickness of a diffusive gel layer at the reactive interface (DGT [43-47]).

Herein we review the available theory for determination of the thermodynamic and kinetic descriptors of metal complex systems from SSCP curves. The robustness of the interpretation framework is illustrated by experimental data on metal complexes with molecular and nanoparticulate complexants. Mechanisms of association of a free hydrated metal ion, M_{aq}^{z+} (M in short), with molecular ligands, L, are often well understood (e.g. Eigen [48-50]), and theoretical frameworks for determination of quantitative metal binding parameters for ML systems from electrochemical data are well established, e.g. stability constants can be determined from the shift in voltammetric half-wave potential in the presence of complexing agents. Kinetic features such as rate constants for association/dissociation and so-called labilities of metal complex species can be characterized by invoking the reaction layer concept [51-54]. The available theory includes accounting for the effects of the diffusion coefficient of ML relative to that of the free M [55-60], ligand protonation [61-64], complex stoichiometry [65,66], and mixtures of ligands [67-71].

The physicochemical reactivity of nanoparticles (NPs) is of great current interest in many scientific and societal domains. In environmental context, the interaction of trace metals with natural and engineered NPs generally affects the speciation and the ensuing bioavailabilities of both the metal ions and the NPs [72-77]. The various types of NPs encompass hard (impermeable) NPs such as silica and metal oxides, core-shell NPs comprising an impermeable core surrounded by a soft shell, and soft (permeable) NPs such as natural organic matter. The particle body often contains charged sites and/or functional groups that can associate with metal ions via electrostatic and/or covalent chemical binding. Electrochemical techniques offer powerful tools for characterising such interactions. Nevertheless, quantitative interpretation of the experimental data generally requires accounting for a number of features of the M-NP system [77-82], including (i) the (much) lower diffusion coefficient of the M-NP species as compared to that of the free metal ion, (ii) the local nature of the complexation on/within the particle surface/body, and thus (iii) the necessary coupling of local particulate processes of association/dissociation and diffusion to/from the particle body with the more macroscopic fluxes in case of the presence of a sensor/medium interface, and

(iv) the possible exclusion effects of NP body volume from the reaction layer at such a macroscopic interface. We note that these considerations apply to implementation of any dynamic speciation technique. Still, electrochemical tools are advantageous because they are inherently not restricted to limiting flux conditions (see above). Furthermore, characterisation of M-NP systems by techniques such as DGT which employ a diffusive gel layer at the sensor/medium interface is confounded by the extent to which nanoparticulate species penetrate the interfacial region and the timescale thereof [83-89].

2. Basic electrochemical features of SSCP (metal-only case)

The recording of a single SCP measurement involves two steps, namely a deposition step during which metal ions in the aqueous solution, M_{aq}^{z+} (M for short), are reduced at a constant potential and accumulate in the form of M^0 in the electrode, followed by a stripping (quantification) step in which the accumulated M^0 is reoxidised by a constant oxidising current, I_s. The analytical signal, τ, is the time taken for reoxidation which is readily obtained from the area under the peak in the dt/dE vs E plot, where dt/dE is the inverse of the time derivative of the recorded potential [90]. During the reoxidation step, M^0 diffuses from the bulk of the electrode to the electrode/solution interface. If the change in electrode potential is faster than the timescale required for diffusion of the M^0 in the electrode volume to maintain the mean concentration M^0 in the bulk of the electrode $\bar{c}_{M^0}$ approximately equal to the concentration of M^0 at the electrode surface $c^0_{M^0}$ (as dictated by the imposed constant current), then the accumulated M^0 may not be completely removed from the electrode during the reoxidation step. In contrast, when the oxidising current is sufficiently low, there is sufficient time for $\bar{c}_{M^0} \approx c^0_{M^0}$ to be maintained over almost the entire reoxidation period (except for the initial and very final stages) [27]. As a consequence, the accumulated M^0 is quantitatively oxidised from the electrode. This so-called complete depletion regime has a number of particularly attractive features. For example, the product $I_s\tau$ is constant and quantification of M^0 accumulated in the electrode during the deposition step corresponds to straightforward application of Faraday's law, i.e.:

$$I_s\tau = \bar{c}_{M^0} nFV_{el} \quad \text{[C]} \quad (1)$$

where V_{el} is the accumulating electrode volume, and other symbols have their usual meaning. Notably the capacitive charging current is effectively eliminated from the signal since it corresponds to the area under the *baseline* of the dt/dE vs E plot [90]. Furthermore, even if secondary effects impact on the shape of the dt/dE vs E curve, so long as there are no interfering faradaic processes and no noticeable changes in the capacitive current in the transition region, τ will correctly quantify the M^0 accumulated during the deposition step. Finally, since $c^0_{M^0} \approx \bar{c}_{M^0}$ throughout practically the entire stripping step, the need to formulate the flux or concentration gradient of M^0 in the electrode volume is circumvented. This effective getting around part of the Nernstian extension of the reoxidation process also leads to greater peak resolution in multi-metal systems compared to non-depletive voltammetric modes. This feature is due to the self-optimising nature of the effective potential scan rate in the depletive mode. That is, during the reoxidation step the potential is controlled by the surface concentration ratio $c^0_M / c^0_{M^0}$ (where c^0_M is the

concentration of metal ion at the medium side of the electrode/medium interface); it is only once $c^0_{M^0}$ ($\approx \bar{c}_{M^0}$) reaches essentially zero, and can no longer carry the imposed current, that the potential will change rapidly until becoming controlled by the oxidation of a less electropositive metal. Nevertheless, the potential-time characteristic of a single SCP curve is quite complicated and relating the stripping peak potential, E_p, and peak half-width, $w_{1/2}$, to metal speciation in the sample solution is not straightforward [24,27]. Complete SSCP waves, i.e. curves constructed from depletive SCP τ values recorded as a function of E_d, overcome difficulties associated with interpretation of E_p and $w_{1/2}$ values for individual SCP curves. The only information taken from each individual SCP curve is the peak area, i.e. τ, which is quantitatively linked to the amount of metal accumulated in the electrode during the deposition step (Eq. (1)). The rigorous equation that fully describes the SSCP wave in the complete depletion range is given by [91]:

$$\tau = \frac{I_d^* \tau_d}{I_s}[1 - \exp(-t_d / \tau_d)] \quad \text{[s]} \quad (2)$$

where I_d^* is the limiting value of the deposition current, t_d is the deposition time, and τ_d is the potential-dependent characteristic time constant of the deposition process [91]:

$$\tau_d = \frac{V_{el}(1/\delta_M + 1/r_0)^{-1}}{A_{el} D_M c^0_M / c^0_{M^0}} \quad \text{[s]} \quad (3)$$

where V_{el} is the electrode volume and A_{el} its surface area. I_d^* is attained when the concentration of metal ion at the electrode surface, c^0_M, is zero, i.e. at sufficiently negative overpotentials:

$$I_d^* = nFA_{el} D_M c^*_M (1/\delta_M + 1/r_0) \quad \text{[A]} \quad (4)$$

where D_M is the diffusion coefficient of the free metal ion, c^*_M is the free metal ion concentration in the bulk aqueous solution, δ_M is the thickness of the aqueous diffusion layer, and r_0 is the radius of the assumed spherical electrode. The limiting value of the transition time, τ^*, is attained in the plateau of the SSCP wave ($E_d << E^0$; $c^0_M / c^0_{M^0} \rightarrow 0$) and corresponds simply to the charge balance for complete depletion [91]:

$$\tau^* = I_d^* t_d / I_s \quad \text{[s]} \quad (5)$$

Use of Eq. (5) implies that the concentration of oxygen and other potential oxidants in solution is sufficiently low so that the rate of oxidation of M^0 is governed solely by I_s. For in-situ measurements, the use of thin film mercury electrodes enables depletive conditions to be achieved at relatively high I_s, thereby avoiding the need for deoxygenation of the sample [92]. We note that in multi-metal solutions the phenomenon of electroless reoxidation in the ongoing stripping step, i.e. oxidation of a given metal by the incoming flux of less electropositive metal ions, may occur but it is unlikely to be relevant under typical environmental conditions [93].

Considering the case of a reversible electron transfer reaction with a Nernstian relationship between the surface concentrations of M and M^0, during application of the deposition potential, E_d:

$$E_d = E^0 + (RT/nF)\ln(c^0_M / c^0_{M^0}) \quad [V] \quad (6)$$

which can be written in terms of the surface concentration ratio:

$$c^0_M / c^0_{M^0} = \exp[nF(E_d - E^0)/RT] \quad (7)$$

The SSCP curve lies at considerably more negative potentials than a conventional dc-voltammogram. This feature is a consequence of the magnitude of the equilibrium potential, E_0^{eq}, that holds at the end of the deposition step, immediately prior to application of I_s, i.e.:

$$E_0^{eq} = E^0 + (RT/nF)\ln(c^*_M / \bar{c}_{M^0}(0)) \quad [V] \quad (8)$$

where $\bar{c}_{M^0}(0)$ is $\bar{c}_{M^0}$ at the end of the deposition step, the magnitude of which is governed by E_d. For given experimental conditions (e.g. t_d, c^*_M), SSCP curves recorded with a microelectrode lie at more negative positions on the E_d axis as compared to those measured with a macroelectrode [27]. This feature is due to the greater $\bar{c}_{M^0}$ in the microelectrode volume (cf. Eq. (8)).

In the case of electrochemically irreversible systems, Eq. (2) also holds, albeit that the expressions for I_d^* and τ_d are more involved [94]. Indeed, SSCP enables irreversibility to be overcome to some extent, and this effect is even greater at a microelectrode. The feature is due to the aforementioned more negative location of the SSCP curves on the potential axis: for more negative E_d values the relative influence of irreversibility on limitation of the deposition current decreases, in line with conventional concepts. That is, irreversibility is lost mostly near the onset of the wave. The dependence of reversibility on $\bar{c}_{M^0}$, and thus on the deposition time and electrode volume, allows this phenomenon to be unambiguously distinguished from other effects that may affect the shape of the SSCP wave, as elaborated in the following sections.

The above treatment considers M^{z+}_{aq} to be the electroactive form of M. We note that the reduction step, $M^{z+}_{aq} + ze^- \rightarrow M^0$, involves dehydration of the metal ion [95]. Accordingly, hydrolysed forms of M will also contribute to the accumulation rate of M^0: the rate of removal of water from the inner-sphere hydration layer typically increases as the degree of hydrolysis increases [50]. We highlight that the theoretical framework is generally applicable to any redox active species that can be accumulated and recovered from an electrode surface. In most cases to date, the accumulation step involves reduction of a metal ion to form an amalgam with a mercury electrode, followed by an oxidative stripping step. The approach has also been demonstrated for metal speciation measurements at a solid bismuth electrode [96], and reductive stripping can be envisaged when an oxidised form of the analyte is adsorptively accumulated [97,98].

3. Metal ion complexes with molecular ligands, ML

SSCP waves enable straightforward interpretation of a wide variety of ML systems. For example, the shift in half-wave (deposition) potential as well as the effect of a reduced diffusion coefficient for ML compared to M can be treated in a manner analogous to the DeFord-Hume expression for voltammetric waves [99-102]. In the following sections we detail the capabilities of SSCP for determining metal binding parameters for molecular and nanoparticulate complexants. Due to the aforementioned features of the complete depletion regime, SSCP waves overcome limitations associated with analogous curves constructed on the basis of SV measurements [30].

We first discuss the simplest case of fully labile metal complexes ML with molecular ligands. In describing the chemodynamic behaviour of metal complexes, it is necessary to define the features at two levels [103,104]. Firstly, at the level of a volume complexation reaction, distinction is made between dynamic and inert systems. A system is denoted as dynamic if there is frequent interchange between free M^{2+}_{aq} in the bulk medium and the complex ML on the timescale of interest, *t*, i.e.:

$$k_a c^*_{L,t} t >> 1 \quad \text{and} \quad k_d t >> 1 \tag{9}$$

where k_a and k_d are respectively the association and dissociation rate constants of the molecular complexation/dissociation reaction (see section 4 for extension to nanoparticulate complexants), and $c^*_{L,t}$ is the total concentration of the reactive form of the molecular ligand in the bulk solution, e.g. the fully deprotonated form [61]. At the other extreme, a system is denoted as inert if there is no significant re-equilibration in response to change in species concentrations in the medium, i.e.

$$k_a c^*_{L,t} t << 1 \quad \text{and} \quad k_d t << 1 \tag{10}$$

Then, at the level of an ongoing process at a reactive surface, dynamic systems are further classified in terms of their lability. The concept of lability describes the interplay between diffusive mass transport and association/dissociation kinetics of metal complexes in the context of an ongoing process at a macroscopic interface, e.g. in the present context of an electrodic process, reduction of the free metal ion at the electrode surface and reoxidation of the accumulated metal to metal ions in the medium. By definition, a fully labile complex is able to maintain equilibrium with the free metal ion at all applicable scales in space and time.

3.1 Labile metal complexes with $D_{ML} \approx D_M$

Consider first the simplest case of a labile 1:1 metal complex, ML, for which the diffusion coefficient of the complex, D_{ML}, is equal to that of the free metal ion, D_M, and the electron transfer reaction is reversible. In such case I^*_d is the same as for the equivalent metal-only case, and τ_d now reflects the rate at which $\bar{c}_{M^0}$ is attained in the presence of L. At the medium side of the electrode/medium interface, $c^0_M / c^0_{M,t} = (1 + K_{ML} c^0_L)^{-1} = (1 + K'_{ML})^{-1}$, where K_{ML} is the stability constant for ML, c^0_L is the concentration of L at the electrode surface ($\approx c^*_{L,t}$ under the typical conditions of excess L over M), and $K'_{ML} = K_{ML} c^0_L$. Thus we can write:

$$c^0_{\mathrm{M}} / c^0_{\mathrm{M}^0} = (1 + K'_{\mathrm{ML}})^{-1} (c^0_{\mathrm{M,t}} / c^0_{\mathrm{M}^0}) \quad (11)$$

and

$$E_{\mathrm{d}} = E^0 - (RT/nF)\ln(1 + K'_{\mathrm{ML}}) + (RT/nF)\ln(c^0_{\mathrm{M,t}} / c^0_{\mathrm{M}^0}) \quad \text{[V]} \quad (12)$$

The full SSCP wave is described by the expression derived for the metal-only case, Eq. (2), albeit with the contributing terms modified according to Eqs. (11) and (12). The ability of Eq. (2) to describe the SSCP wave for a simple, labile complex system is illustrated in Fig. 1 for the case of Cd(II) complexes with pyridine-2,6-dicarboxylic acid (PDCA).

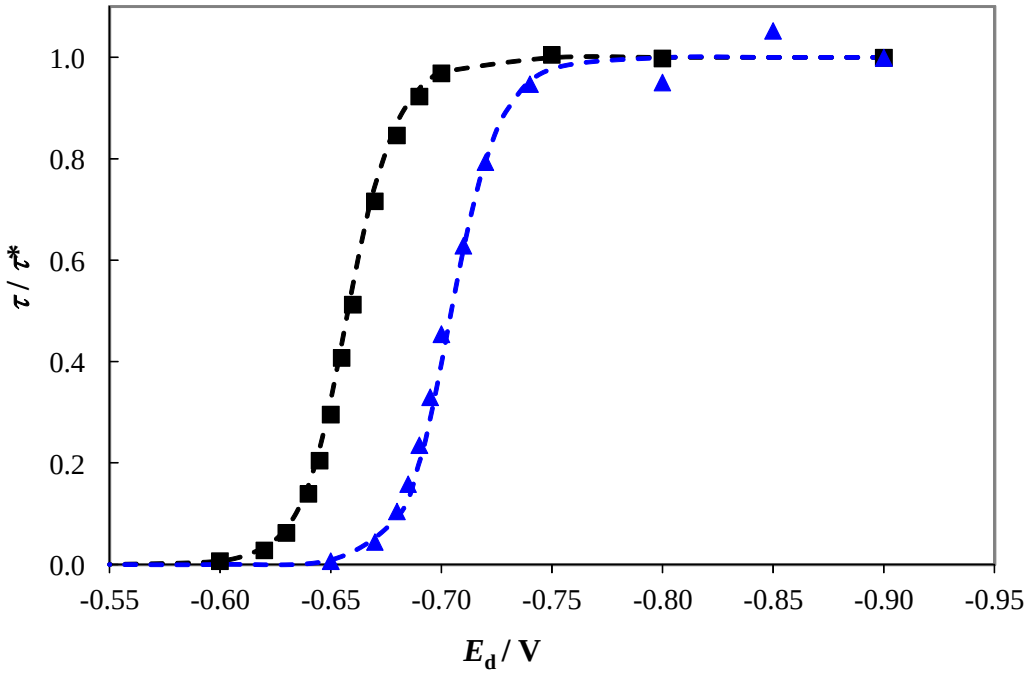

Fig. 1. SSCP curves for Cd(II) only (black symbols and curves) and Cd(II) in the presence of pyridine-2,6-dicarboxylic acid (PDCA; blue symbols and curves). Experimental data are shown as points and calculated values correspond to the dashed curves. Measurements were made at a hanging mercury drop electrode at pH 5 in 100 mol m^{-3} KNO_3, with a total Cd(II) concentration of 2×10^{-4} mol m^{-3} and total PDCA concentration of 10^{-2} mol m^{-3}, 66% of which is present as L^{2-} at pH 5 [105]. Other parameters: I_s = 2 nA, t_d = 300 s, $D_{Cd} = D_{CdPDCA}$ = 7 x 10^{-10} m^2 s^{-1} [106], A_{el} = 5.2 × 10^{-7} m^2, V_{el} = 3.5 × 10^{-11} m^3, log K_{CdPDCA}= $10^{3.75}$ m^3 mol^{-1} [105]. Figure is adapted from ref. [99].

Equation (2), with the pertaining expressions for I^*_{d} and τ_{d}, has been shown to correctly describe the SSCP wave in a range of metal complex systems, including those involving electrochemical irreversibility [94,107], kinetic currents [108-110], induced metal adsorption [99,111], and chemical heterogeneity [29,112,113]. In the case of chemically heterogeneous ML, the stronger complexes of ML are being dissociated towards the plateau of the wave (see section 4.3. below). In the foot of the SSCP wave, when the deposition time is sufficiently long for $\bar{c}_{\mathrm{M}^0}$ to attain its equilibrium value at the applied E_{d}, the analytical signal represents the free metal ion concentration in the bulk solution.

3.2 Labile complexes with $D_{ML} < D_M$

When the diffusion coefficient of the metal complex species is significantly lower than that of the free metal ion, then the analytical signal for labile ML will be smaller than that for the equivalent metal-only case. This factor is accounted for in the expression for the deposition current by replacing D_M with the average diffusion coefficient of the metal in the presence of a complexant, $\overline{D}$:

$$\overline{D} = \frac{D_M c_M^* + D_{ML} c_{ML}^*}{c_{M,t}^*} \qquad [m^2\ s^{-1}] \qquad (13)$$

The corresponding diffusion layer thickness, $\overline{\delta}$, reflects the hydrodynamic conditions, e.g. for effectively laminar flow, $\overline{\delta} = \delta_M / (D_M / \overline{D})^{1/3}$ [114]. The deposition step in SCP is the same as that for SV, and thus the magnitude of $\overline{\delta}$ has the same sensitivity to $\overline{D}$ and the hydrodynamic conditions, as discussed in the literature [57,115-117]. The characteristic time constant, τ_d, becomes [99]:

$$\tau_d = \frac{V_{el}(1/\overline{\delta} + 1/r_0)^{-1}}{A_{el}\overline{D}c_M^0 / c_{M^0}^0} \qquad [s] \qquad (14)$$

It follows from Eq. (14) that a decrease in $\overline{D}$ will increase τ_d and shift the position of the SSCP wave to more positive potentials on the E_d axis. This feature is in line with conventional voltammetric behaviour of metal complexes [1,55,57].

3.3 Kinetic current regime

When metal complex species are not fully labile on the timescale of interest, the dissociation rate of ML partly determines the contribution of the complex to the interfacial metal ion flux. In this regard the approximative Koutecký-Koryta (KK) scheme [51-54,118,119] has been shown to have great utility for describing the lability of molecular complexes in a wide range of circumstances [63,70,109]. The KK approximation divides the concentration profiles of free and complexed M in the diffusion layer into a labile and nonlabile region, separated by the boundary of the so-called reaction layer (Fig. 2). The thickness of the reaction layer, λ, i.e. the distance that the nonlabile region extends from the reactive surface into the surrounding medium, derives from the mobility of free M in the bulk aqueous solution, D_M, and its mean free lifetime, $1/k_a c_{L,t}^*$, together with the mobility of the complex, D_{ML}, and the mean free lifetime of the complex species ML, $1/k_d$ [35,39]:

$$\lambda = \left(\frac{k_a c_{L,t}^*}{D_M} + \frac{k_d}{D_{ML}} \right)^{-1/2} \qquad [m] \qquad (15)$$

For molecular complexants, $k_a = k_w K^{os}$, where k_w is the inner-sphere dehydration rate constant of the hydrated metal ion and K^{os} is the stability constant of the outer-sphere association between the hydrated metal ion and L which is estimated on the basis of ion pair electrostatics [120]; $k_d = k_a/K_{ML}$. Within the basic KK scheme, the contribution from ML to the interfacial metal ion flux is purely kinetic, just like in

the treatment by Heyrovský/Kůta for the case of $K'_{ML} >> 1$ [51]. We note that the original formulation of the reaction layer considered only dissociation of very strong complexes ML with $(D_{ML} / D_M)K'_{ML} >> 1$, in which case Eq. (15) reduces to the familiar expression for the dissociation reaction layer $\mu = (k_a c^*_{L,t} / D_M)^{-1/2}$ [51-53]. Throughout the text herein, our use of the term "reaction layer" refers to the more general definition given by Eq. (15).

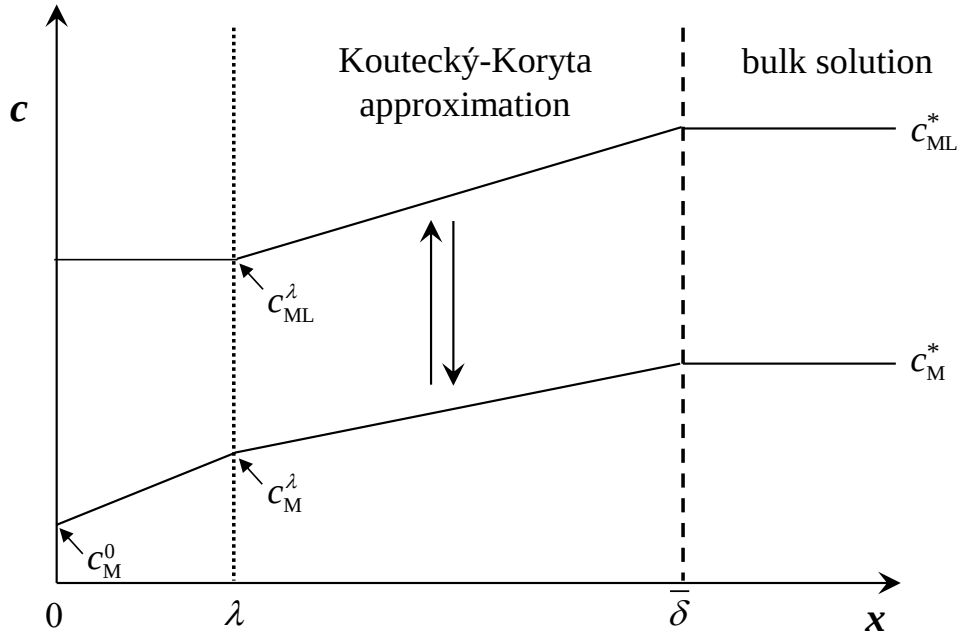

Fig. 2. Schematic concentration profiles, according to the Koutecký-Koryta (KK) approximation, established at the electrode/medium interface (at which M^{z+} is reduced) in a solution containing free metal ions, M, and complexes with a molecular ligand, ML, as a function of distance, *x*, from the electrode surface (at $x = 0$). Arbitrary thicknesses are shown for the reaction layer, λ, and the mean diffusion layer for M and ML, $\bar{\delta}$. The concentrations of M and ML at the reaction layer boundary are denoted by c^λ_M and c^λ_{ML}, respectively. The KK approximation specifies that equilibrium is maintained between M and ML from the bulk solution until $x = \lambda$. Figure is adapted from ref. [108].

The so-called lability parameter is defined as the ratio between the kinetic and diffusive fluxes [35,39]. The kinetic flux, J_{kin}, represents the maximum rate at which ML dissociates to release free M:

$$J_{kin} = k_d c^*_{ML} \lambda \qquad [\text{mol m}^{-2}\,\text{s}^{-1}] \qquad (16)$$

The limiting purely diffusive flux, J^*_{dif}, represents the maximum rate at which the complex species of M arrive at the outer boundary of the steady-state diffusion layer:

$$J^*_{dif} = \frac{\bar{D} c^*_{M,t}}{(1/\bar{\delta} + 1/r_0)^{-1}} \qquad [\text{mol m}^{-2}\,\text{s}^{-1}] \qquad (17)$$

The lability parameter, $\mathcal{L}$, is given by:

$$\mathcal{L} = J_{kin} / J^{*}_{dif} \quad (18)$$

It follows that for a labile complex, $\mathcal{L} >> 1$.

In the kinetic case, the expression for the SSCP wave, Eq. (2), still holds, albeit that the pertaining expressions for I_d^* and τ_d are modified to include the lability parameter as detailed previously [108]. In the kinetic case, I_d^* and τ^* are smaller, and τ_d is larger as compared to the fully labile case. Notably the shape of the SSCP wave for the kinetically controlled case is the same as that for free metal ion only, and the stability constant can still be obtained from the shift in half-wave deposition potential, $E_{d,1/2}$, by including a term that accounts for the positive shift in the wave position due to the reduced lability (lower τ^*) as detailed in previous work [108,121]. The ability of Eq. (2) to describe the SSCP wave in the kinetic current regime is illustrated in Fig. 3 for the well-known case of Cd(II) complexes with nitrilotriacetic acid (NTA) [108,122-124]. The data in Fig. 3 were recorded with a conventional hanging mercury electrode; the lability is lower at a microelectrode [108] due to enhanced diffusion, *cf.* Eq. (18) [40,41].

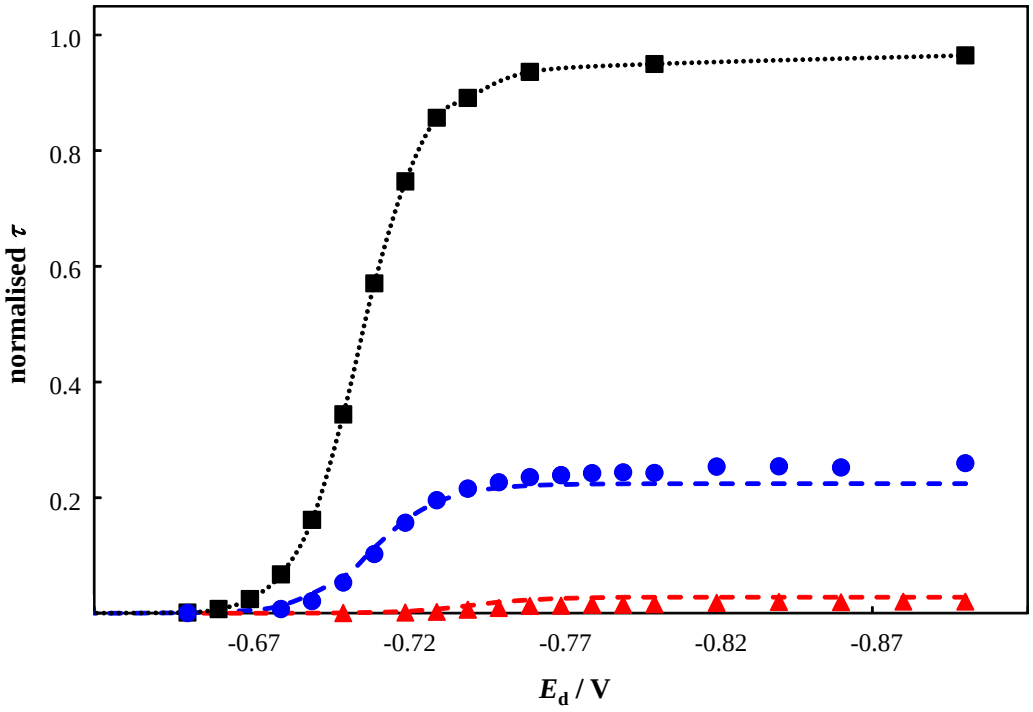

Fig. 3. Comparison of experimental and calculated SSCP waves for Cd(II) complexes with nitrilotriacetic acid (NTA) at pH 8. Experimental data (points) were measured with a hanging mercury drop electrode (t_d 180 s) for 2 x 10^{-4} mol m^{-3} Cd(II) (■) and in the presence of NTA at a total concentration of 10^{-3} mol m^{-3} (●) and 0.1 mol m^{-3} (▲). At pH 8, *ca.* 10% of the total NTA is present as L^{3-} [125], thus calculated curves correspond to the kinetic case for free L^{3-} concentrations of 10^{-4} mol m^{-3} (blue dashed line) and 10^{-2} mol m^{-3} (red dashed line), using the parameters $K_{CdNTA} = 10^{6.8}$ m^3 mol^{-1} [126], $D_{Cd} = D_{CdL} = 7 \times 10^{-10}$ m^2 s^{-1} [106], A_{el} = 5.2 × 10^{-7} m^2, $V_{el} = 3.5 \times 10^{-11}$ m^3, $\delta = 6 \times 10^{-5}$ m, $k_W(Cd) = 3 \times 10^8$ s^{-1} [50]. The reaction layer thickness

was computed taking into account the protonated forms of the ligand [61]. Data are normalised with respect to τ^* for the labile case. Figure is calculated from data published in ref. [108].

It is evident from the preceding discussion that any description of the lability of metal species must be coupled with specification of the effective timescale. In the case of electrochemical stripping techniques, the operational timescale derives from the applicable spatial scale, e.g. the aqueous diffusion layer thickness at a conventional electrode or the radius of a microelectrode, and the pertaining (average) diffusion coefficient of the metal species. The operational timescale can be varied by manipulation of the hydrodynamic conditions, e.g. rate of stirring of the solution or rotation of the electrode, and by changing the size of the electrode [114,127]. For $D_{ML} \approx D_M$, typical accessible timescales are of the order of 10 s at a conventional hanging mercury drop electrode and of the order of ms at a microelectrode. In comparison, DGT with a typical diffusive gel layer thickness of *ca.* 1 mm has an operational timescale of order 10^3 s.

4. Metal complexes with nanoparticulate complexants, M-NP

4.1. Reactivity features of M-NP complexes in bulk dispersion

In recent years, the special metal ion complexation features of nanoparticulate ligands have been delineated, and the underlying physicochemical theory has been developed to include the chemodynamic characteristics of nanoparticulate metal complexes [78-82]. A leading feature of nanoparticulate complexants is the spatial confinement of the metal ion binding sites to the particle surface (in the case of hard, impermeable particles) or to the particle volume (in the case of soft, permeable particles, and in part for core-shell nanoparticles). Thus, the metal ions have to diffuse from the surrounding medium to the individual particles before complexation can occur. Furthermore, the complexation must be interpreted in terms of the *local* conditions prevailing within the particle body, e.g. reactive site density, charge density, ionic strength, pH. It is thus fundamental to distinguish between smeared-out concentrations, *i.e.* conventional concentrations for chemical species averaged over the entire volume of the dispersion, *vs*. the local intraparticulate species concentrations. Herein we discriminate between local, intraparticulate concentrations of a given species *i*, denoted by c_i, and corresponding smeared-out concentrations, denoted by $\bar{c}_i$; bulk free ion concentrations are denoted by c_i^*.

The elaborated Eigen scheme for metal complexation by NPs is shown in Fig. 4. Any one of the given steps may be rate-limiting for the overall association or dissociation reaction. Expressions are available for the pertaining association and dissociation rate constants shown in Fig. 4, for all types of NPs (hard, core-shell, soft) [78-82]. For convenience, we briefly summarise below the expressions for an aqueous highly charged spherical soft NP with particle radius, r_p, larger than the intraparticulate Debye length, κ_p^{-1}, i.e. $\kappa_p r_p > 1$ [128,129]. The reader is referred to previous work for the detailed derivations of the expressions and the pertaining modifications for other types of NPs [78-82,130-133].

In the association step, the limiting rate of diffusive supply of M^{z+} towards a spherical NP, per reactive site S, can be generally written as [80,81]:

$$R_{a,p} = 4\pi N_{Av} r_p D_M \overline{f}_{el,a} c_M^* \overline{c}_{S,t} / N_S \qquad [\text{mol m}^{-3}\ \text{s}^{-1}] \qquad (19)$$

with corresponding rate constant:

$$k_{a,p} = 4\pi N_{Av} r_p D_M \overline{f}_{el,a} / N_S \qquad [\text{m}^3\ \text{mol}^{-1}\ \text{s}^{-1}] \qquad (20)$$

where $\overline{c}_{S,t}$ is the total smeared-out concentration of the reactive form of S per unit volume of dispersion (e.g. deprotonated form), N_S is the number of S per particle; and $\overline{f}_{el,a}$ is the electrostatic coefficient for conductive diffusion towards the NP. The limiting rate of inner-sphere complexation, for the situation in which the Boltzmann distribution of charged species between the bulk medium and the NP body is at equilibrium, is given by [80,81]:

$$R_a^{is} = k_w V^{os} \overline{f}_B N_{Av} c_M^* \overline{c}_{S,t} \qquad [\text{mol m}^{-3}\ \text{s}^{-1}] \qquad (21)$$

with corresponding rate constant:

$$k_a^{is} = k_w V^{os} \overline{f}_B N_{Av} \qquad [\text{m}^3\ \text{mol}^{-1}\ \text{s}^{-1}] \qquad (22)$$

where k_w is the rate of inner-sphere dehydration of the metal ion, V^{os} is the outer-sphere volume per site S, and $\overline{f}_B$ is the Boltzmann equilibrium factor for the partitioning of the free metal ion M^{2+} between medium and particle body.

In the dissociation step, the limiting rate of diffusion of released M^{z+} from the spherical NP into the medium is generally given by [81]:

$$R_{d,p} = \frac{3 D_M \overline{f}_{el,d}}{r_p^2 \overline{f}_B} \overline{c}_M \qquad [\text{mol m}^{-3}\ \text{s}^{-1}] \qquad (23)$$

where $\overline{f}_{el,d}$ is the coefficient for conductive diffusion from the NP into the bulk medium (i.e. beyond the outer border of the diffusion layer as shown in Fig. 5) and $\overline{c}_M$ is the smeared-out concentration of intraparticulate free metal ion. The corresponding diffusion-controlled rate constant for the release of M, $k_{d,p}$, is given by:

$$k_{d,p} = 3 D_M \overline{f}_{el,d} (1 + K_{int} c_{S,t}) / r_p^2 \overline{f}_B \qquad [\text{s}^{-1}] \qquad (24)$$

where K_{int} is the conventional intrinsic stability constant of the inner-sphere complex, expressed in terms of the *intraparticulate* concentrations of the free metal ion, c_M, inner-sphere complexes, c_{MS}, and total concentration of the reactive form of the binding sites, $c_{S,t}$, i.e. [77,134]:

$$K_{int} = c_{MS} / \left[c_M (c_{S,t} - c_{MS}) \right] \qquad [\text{m}^3\ \text{mol}^{-1}] \qquad (25)$$

The limiting rate of dissociation of inner-sphere complexes, MS, is given by [81]:

$$R_{\mathrm{d}}^{\mathrm{is}} = \frac{k_{\mathrm{a}}^{\mathrm{is}}}{K_{\mathrm{int}}\,\overline{f}_{\mathrm{B}}} c_{\mathrm{MS}} \qquad [\mathrm{mol\ m^{-3}\ s^{-1}}] \qquad (26)$$

where $k_{\mathrm{a}}^{\mathrm{is}}$ is given by Eq. 22 and c_{MS} is the *intraparticulate* concentration of MS. The rate constant for inner-sphere dissociation, $k_{\mathrm{d}}^{\mathrm{is}}$, follows as [81]:

$$k_{\mathrm{d}}^{\mathrm{is}} = k_{\mathrm{a}}^{\mathrm{is}} / K_{\mathrm{int}}\,\overline{f}_{\mathrm{B}} = k_{\mathrm{w}} V^{\mathrm{os}} N_{\mathrm{Av}} / K_{\mathrm{int}} \qquad [\mathrm{s^{-1}}] \qquad (27)$$

The overall release of M from the particle body involves consecutively dissociation of inner-sphere MS followed by diffusion of the ensuing M^{2+} from the particle into the surrounding medium (Figs. 4 and 5). Accordingly, the rate-limiting step can be governed by either $k_{\mathrm{d}}^{\mathrm{is}}$ or $k_{\mathrm{d,p}}$. In the present context of highly charged soft NPs, we consider particles with a substantial water content, in which case diffusion into the particle body is usually fast in comparison to extraparticulate diffusion in the aqueous medium [127].

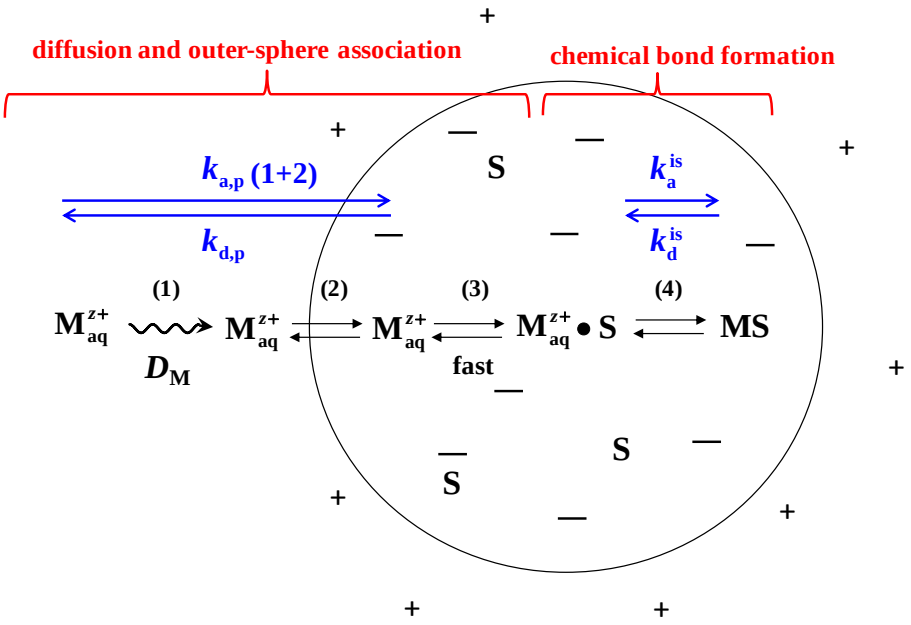

Fig. 4. Steps involved in the associative and dissociative interaction of an aqueous charged metal ion, M_{aq}^{z+}, (z is the charge number) with a spherical soft nanoparticle containing charged or uncharged reactive sites (S) and charged indifferent sites (–). The +'s denote the counterions accumulated in the extraparticulate part of the (nominally negative) particle electric field, and the k's represent the pertaining rate constants. The associative steps are (1) diffusion of M_{aq}^{z+} from the bulk solution to the surface of the nanoparticle, (2) incorporation within the particle body as a free hydrated ion, (3) outer-sphere association of M_{aq}^{z+} with S, to form M_{aq}^{z+}•S, and (4) formation of a covalent chemical bond, MS, which generally follows upon the release of water from the inner hydration layer by M_{aq}^{z+}. Figure is reproduced from ref. [135].

4.2. Lability of M-NP complexes at a reactive interface

Conventional criteria for lability implicitly assume that the dimensions of the complexing ligand are on the molecular scale with dimensions always smaller than the thickness of the reaction layer [51-54,118,119]. In

the case of dispersed nanoparticulate metal complexes, the notion of lability involves the frequency of exchange of M between M_{aq}^{z+} in the bulk medium and MS within the particle body. In the context of an ongoing process at a reactive macroscopic interface, formulation of the lability parameter for M-NP species inherently requires connecting the chemodynamic features of M-NP entities at the local level (intraparticulate association/dissociation kinetics and diffusion to/from the particle body) with macroscopic fluxes at reactive interfaces [77,82,135-138]. In this regard we highlight that the notion of a conventional reaction layer only has meaning in the presence of a finite amount of complexing sites, S (see Section 3.1.3, Eq. 15). Accordingly, the use of reaction layer concepts to describe the chemodynamic features of M-NP entities requires distinction between (i) a conventional intraparticulate reaction layer, with thickness λ_{NP}, at the particle side of the NP/medium interface, and (ii) an operational reaction layer, with thickness $\bar{\lambda}$, that is in effect at some macroscopic reactive interface, e.g. an electrode surface (Fig. 5) [77,82,135-138]. The magnitude of $\bar{\lambda}$ derives from the time-averaged presence of the NP body volume and the corresponding time-averaged concentration of S with the operational reaction layer, $\bar{c}_S^{\lambda}$. Analogous to the expression for the molecular case (Eq. 15), we can write [137,138]:

$$\bar{\lambda} = \left(\frac{k_{a,p} \bar{c}_S^{\lambda}}{D_M} + \frac{k_d}{D_p} \right)^{-1/2} \quad \text{[m]} \qquad (28)$$

where k_d is the composite dissociative rate constant, $(1/k_{d,p} + 1/k_d^{is})^{-1}$ [35], and $k_{a,p}$ is the only associative rate constant involved because the relevant timescale is the one for M to enter the volume of the NP body [137,138]. We note that there are fundamental differences between the intraparticulate binding sites, S, and molecular ligands in solution, L, e.g. entropical factors. The relative magnitudes of r_p and $\bar{\lambda}$ have implications for the lability of M-NP species at a reactive interface as discussed below.

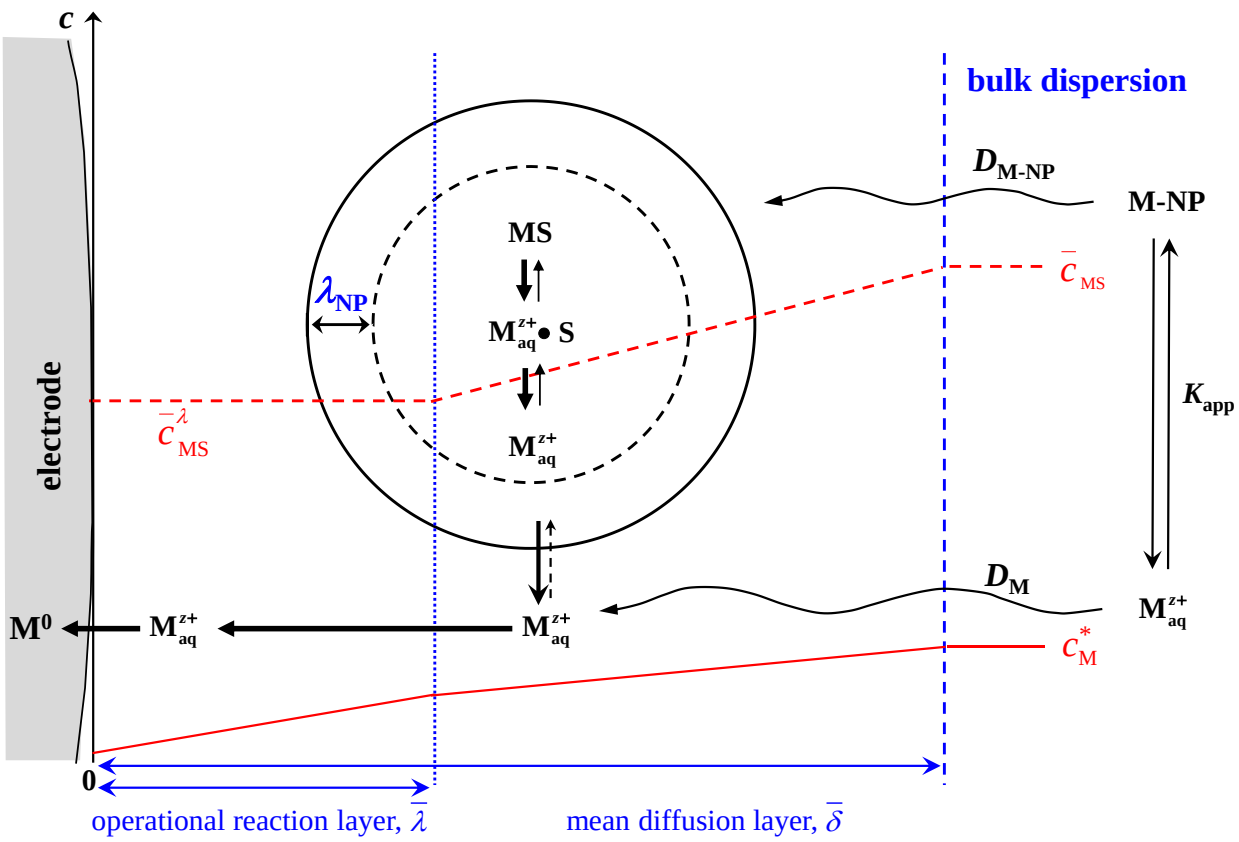

Fig. 5. Schematic view of the processes governing the flux of M, in an aqueous dispersion of nanoparticulate complexes of M, toward an electrode at which free M^{z+}_{aq} is reduced to M^0. The concentration profile of the free M^{z+}_{aq} in the medium, c^*_M, is sketched by the solid red line, and the profile of the average concentration of MS complexes within each spatial zone, $\bar{c}_{MS}$, is indicated by the dashed red line with $\bar{c}^{\lambda}_{MS}$ denoting the average concentration within the operational reaction layer. For clarity, the size of the NP is exaggerated and arbitrary thicknesses are shown for the intraparticulate reaction layer, λ_{NP}, the operational reaction layer at a macroscopic interface, $\bar{\lambda}$, and the mean solution diffusion layer for M^{z+}_{aq} and MS, $\bar{\delta}$. Figure is adapted from Fig. 9 in ref. [77].

Analogous to the rationale described in Section 3.1.3 for molecular ligands, the lability parameter for nanoparticulate MS corresponds to the ratio between the kinetic and diffusive fluxes, $\mathcal{L}_{NP} = J_{kin} / J^*_{dif}$. In the M-NP case, and where intraparticulate diffusion of free M is faster than that in the bulk medium, the rate of release of M^{z+}_{aq} from the NP body into the bulk medium is governed by the rate of chemical dissociation of MS. The kinetic flux, J_{kin}, is thus given by [135]:

$$J_{kin} = k^{is}_d \bar{c}^{\lambda}_{MS} \bar{\lambda} \qquad [\text{mol m}^{-2}\ \text{s}^{-1}] \qquad (29)$$

where $\bar{c}^{\lambda}_{MS}$ is the average concentration of MS within the operational reaction layer zone, $\bar{\lambda}$, at the reactive interface (Fig. 5). The limiting purely diffusive flux, J^*_{dif}, corresponds to the average rate at which all

forms of M diffuse towards the reactive surface; in the M-NP system this includes the free M_{aq}^{z+} in the bulk dispersion and all the intraparticulate forms of M. Thus we can write [135]:

$$J_{dif}^{*} = \overline{D}(c_M^{*} + \bar{c}_{MS} + \bar{c}_M + ...) / (1/\bar{\delta} + 1/r_0)^{-1} \qquad [\text{mol m}^{-2}\ \text{s}^{-1}] \qquad (30)$$

where the intraparticulate forms of M are necessarily expressed as smeared-out concentrations (denoted by the overbar).

It is evident from Fig. 5 that the size of the NP body, r_p, relative to the thickness of the operational reaction layer, $\bar{\lambda}$, will play a role in determining the apparent lability of the M-NP system. That is, under certain conditions, geometrically-controlled exclusion of NP body volume from $\bar{\lambda}$ gives rise to a corresponding lowering in the average concentration of sites inside the reaction layer which affects the properties of the reaction layer itself, Eq. (28), and the overall lability of M-NP systems at the reactive interface, Eq. (29) [135-138]. A general theoretical framework has been developed which delineates the multifactorial rocesses that control the magnitude of M-NP lability parameter at a given reactive interface, i.e. particle size, electrostatic features, density of metal binding sites, dehydration kinetics of the complexing metal ion, and the intrinsic stability of the MS complex [82,137,138]. It was gratifying to find that old voltammetric lability data on Cd(II) complexes with latex nanoparticles [139,140] appeared to be in excellent agreement with those predicted on the basis of the computed $\mathcal{L}_{NP}$, accounting for the reduced NP body volume in $\bar{\lambda}$ [77].

The information presented in the preceding sections identifies SSCP as a powerful tool for application to M-NP systems, i.e. factors associated with the lability features can be unambiguously identified and accounted for in the interpretation. In the fully labile case, the reaction layer is immaterial, and thus the M-NP system can be treated as per the $D_{ML} < D_M$ case discussed in Section 3.1.2. In the kinetic current regime, i.e. $\mathcal{L}_{NP} < 1$, the expressions for I_d^{*} and τ_d are derived by invoking the KK approximation (Section 3.1.3), i.e. assuming a spatially discontinuous transition from labile to non-labile behaviour, as illustrated schematically by the concentration profiles in Fig. 5. The sought expressions follow from those derived previously for the molecular case under the limiting context of the KK approximation, i.e. $(D_{M\text{-}NP} / D_M)K_{int}^{'} >> 1$ [108,109]:

$$I_d^{*} = \frac{nFA\overline{D}c_M^{*}}{(1/\bar{\delta} + 1/r_0)^{-1}} \frac{\left(1 + \overline{K}_{app}\bar{c}_{S,t}\right)}{(1 + 1/\mathcal{L}_{NP})} \qquad [\text{A}] \qquad (31)$$

and

$$\tau_d = \frac{V(1/\bar{\delta} + 1/r_0)^{-1}}{A\overline{D}c_M^0 / c_{M^0}^0} \frac{(1 + 1/\mathcal{L}_{NP})}{(1 + \overline{K}_{app}\bar{c}_{S,t})} \qquad [\text{s}] \qquad (32)$$

where $\mathcal{L}_{NP}$ inherently accounts for geometric exclusion of the NP body from $\bar{\lambda}$ via Eq. (29), and $\overline{K}_{app}$ is the apparent stability constant of the metal-particle associates [77]:

$$\overline{K}_{\mathrm{app}} = \bar{c}_{\mathrm{M,b}} / \left[c_{\mathrm{M}}^{*} (\bar{c}_{\mathrm{S,t}} - \bar{c}_{\mathrm{M,b}}) \right] \qquad [\mathrm{m^3\ mol^{-1}}] \qquad (33)$$

where $\bar{c}_{\mathrm{M,b}}$ is the smeared-out total concentration of all forms of M associated with the nanoparticulate complexant. The overbar notation signifies that $\overline{K}_{\mathrm{app}}$ represents a weighted average of the stabilities over all associated forms of M with the nanoparticulate complexant. $\overline{K}_{\mathrm{app}}$ appears in Eqs. (31) and (32) because the expressions are concerned with coupling the local processes (involving all forms of M associated with the NP) with macroscopic ones. The intrinsic stability of the inner-sphere complexes MS is evidently a contributing factor determining the lability of the M-NP system under the given timescale. The magnitude of K_{int}, Eq. (25), is taken into account via the inner-sphere complex concentration terms in Eqs. (29) and (30). We highlight that the dependence of $\bar{\lambda}$ and $\mathcal{L}_{\mathrm{NP}}$ on r_{p} is rather involved, and the reader is referred to our previous work for details [138]. Geometric exclusion of NP body volume from a macroscopic reaction layer is a general feature of M-NP systems. The window in which the phenomenon is significant for the analytical measurement depends on the interplay between the various features of the M-NP system (r_{p}, charge density, K_{int}) and the target metal ion (k_{w}), together with the timescale of the speciation technique ($\bar{\delta}$, r_0) [82,135-138].

4.3. Chemically heterogeneous nanoparticulate metal complexes

In the case of chemically heterogeneous complexants, the equilibrium relation between M and the various reactive sites is given by a distributed intrinsic affinity. A characteristic feature of such systems is that the effective intrinsic stability constant, $\overline{K}_{\mathrm{int}}$, varies with the degree of occupation of the binding sites, θ_{M}. The overbar notation signifies that $\overline{K}_{\mathrm{int}}$ represents a weighted average of all types of inner-sphere complexes at a given θ_{M}. Chemically heterogeneous complexants are typified by humic substances, which are natural heterogeneous soft charged NPs [1,130,141]. SSCP is a powerful tool for studying such systems because the effective M:S ratio at the electrode interface spans a range of values on going from the foot to the plateau of the wave, i.e. a range of $\overline{K}_{\mathrm{int}}$ and k_{d} values can be probed for a single bulk solution composition [29,112]. The shape of the SSCP wave reflects the chemical heterogeneity in the metal complexation, i.e. the distribution of $\overline{K}_{\mathrm{int}}$ values. On going from the foot to the plateau of the wave, θ_{M} at the electrode surface decreases and thus the locally effective $\overline{K}_{\mathrm{int}}$ increases according to the applicable affinity distribution. Thus the complexation energy is greater at the electrode surface compared with the bulk dispersion, and this difference progressively increases as E_{d} becomes more negative. Consequently, similar to effects observed by conventional voltammetry [2,142-144], in the presence of chemically heterogeneous metal complexes the SSCP wave is spread out along the E_{d} axis. The extent to which the SSCP wave is flattened as compared to the homogeneous case is a measure of the degree of heterogeneity, Γ, of the metal complex system.

Theory has been developed to describe SSCP waves for heterogeneous metal complexes [112]. Taking the Freundlich isotherm as an arbitrary but popular starting point [2], the relationship between the free M and the complexes with all of the site types, S_i, is given by:

$$\sum_i c_{\mathrm{MS}_i} = B(c_{\mathrm{M}})^{\Gamma} \qquad [\mathrm{mol\ m^{-3}}] \qquad (34)$$

where B is a binding affinity parameter and Γ represents the heterogeneity; $0 < \Gamma < 1$; $\Gamma = 1$ in homogeneous case. For labile heterogeneous metal complex systems, the $1+K'$ term in Eq. 12 is replaced by $1+Bc_{\mathrm{M}}^{(\Gamma-1)}$ [112]. Accordingly, the shift in potential along the SSCP wave in the presence of a heterogeneous complexant relative to the metal-only case is given by:

$$\Delta E_{\mathrm{d}} = (RT/nF)\ln(1+Bc_{\mathrm{M}}^{0\,(\Gamma-1)}) - (RT/nF)\ln(\overline{D}/D_{\mathrm{M}})^{p} \qquad [\mathrm{V}] \qquad (35)$$

where c_{M}^{0} is the concentration of free metal ion at the electrode surface (which simply follows from that in the bulk solution and the fractional position along the SSCP wave, as detailed previously [112]), $p = 1$ for a microelectrode and between $\frac{1}{3}$ and $\frac{1}{2}$ for a conventional macroscopic electrode [114].

The measured and computed SSCP waves for an example chemically heterogeneous system, namely Cu(II) and Cd(II) complexes with nanoparticulate humic acid (HA), are shown in Fig. 6. Both curves correspond to labile conditions, i.e. the measured τ^* corresponds to that predicted for the labile case, with accounting for the reduced diffusion coefficient of the metal complex species (section 3.2). The SSCP wave for CuHA is spread along the E_{d} axis to a greater extent than the wave for CdHA, which reflects the greater heterogenity of Cu(II) complexation with HA. The CuHA data correspond to a Γ of *ca*. 0.2, whilst the CdHA data are described by a Γ of *ca*. 0.7 (Fig. 6), in line with the body of literature data on the heterogeneity of metal-humic complexation [1]. We have shown that the Γ value obtained from the shape of an SSCP wave is in good agreement with that obtained from independent measurements of $\overline{K}_{\mathrm{int}}$ as a function of θ_{M} over a range of bulk solution compositions [145-147]: this finding provides strong support for the interpretation framework. Furthermore, the aforementioned features of SSCP mean that chemical heterogeneity can be unambiguously identified and discriminated from other factors that can influence the shape of the wave, e.g. irreversibility. Specifically, for a labile and chemically heterogeneous complex system, the shape of the SSCP wave will be the same at a conventional electrode and at a microelectrode, and will be independent of deposition time [29].

In the kinetic current regime, the applicable expressions for I_{d}^{*} and τ_{d} follow from those given above for the nanoparticulate case, Eqs. (30) and (31). However, rigorous description of the SSCP wave is rather involved because $\overline{K}_{\mathrm{app}}$, $\overline{K}_{\mathrm{int}}$, $\overline{D}$, and the kinetic parameters are functions of distance within the diffusion layer, and changes in these parameters are coupled [112]. Preliminary explorations, based on the KK approximation, resulted in a reasonable description of the SSCP waves in the kinetic regime for moderate degrees of heterogeneity [112]. The greater the degree of heterogeneity, the greater the difference between

the effective chemical affinity in the bulk solution and within the reaction layer, and the more readily lability is lost toward the plateau of the SSCP wave [2,112].

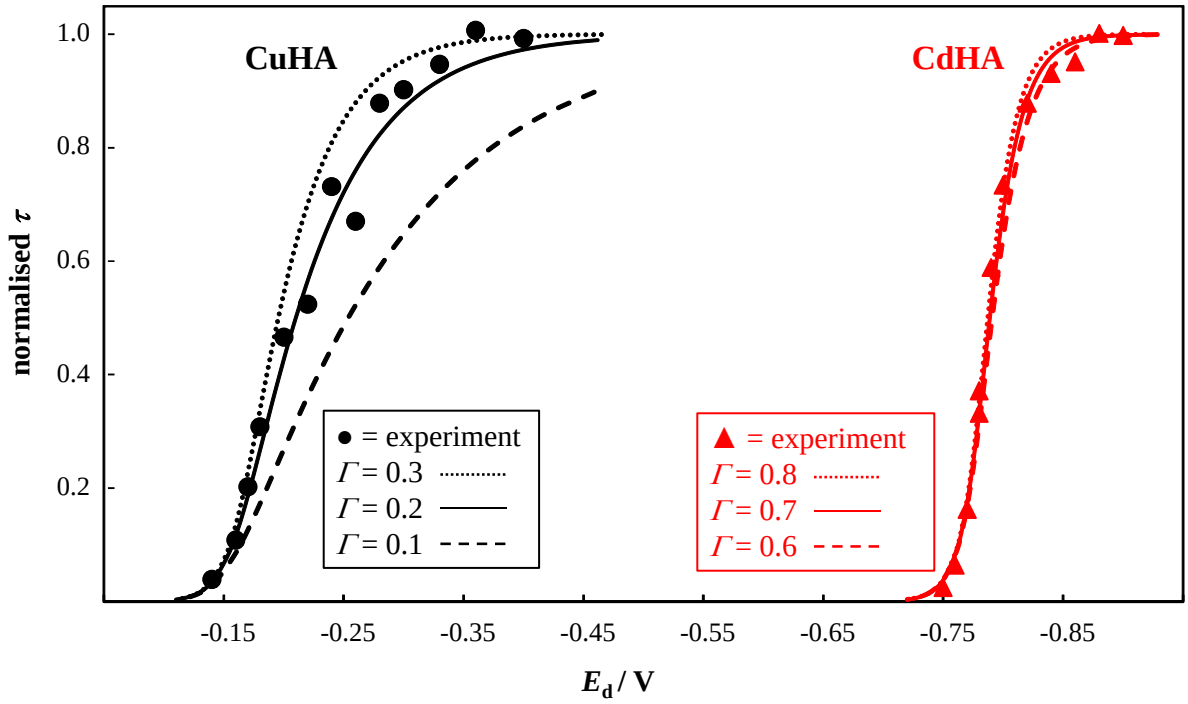

Fig. 6. SSCP waves for labile Cu(II) and Cd(II) complexes with humic acid. Experimental data (points) are shown together with the computed waves (curves) for the Γ values indicated on the figure. Data are normalised with respect to the pertaining τ^*. The experimental data correspond to $\bar{c}_{M,b} / \bar{c}_{S,t} \approx 0.03$ and were measured in $Ca(NO_3)_2$ electrolyte at pH 6 and ionic strength of 100 mol m^{-3} for CuHA and 10 mol m^{-3} for CdHA. Figure is adapted from published data [145].

5. Conclusions and outlook

SSCP in the complete depletion regime is a powerful electrochemical tool that provides comprehensive information on the thermodynamic and kinetic features of metal ion complexes with molecular and nanoparticulate complexants. In common with voltammetric scans, SSCP waves inherently probe a portion of the stability constant distribution and the associated complex formation/dissociation rate constant distribution. This characteristic is a major advantage over other non-equilibrium techniques which are typically configured to measure only under limiting steady-state flux conditions. Another notable feature of the complete depletion regime of SSCP is that it provides a quantitative measure of the metal accumulated in the electrode during the deposition step, which is a major advantage over non-depletive stripping voltammetric methods. Features of SSCP that render the technique particularly advantageous for metal speciation analysis in environmental and biological matrices include its insensitivity to induced metal adsorption, and ability to unambiguously discriminate between various factors that can influence the shape of the waves, e.g. electrochemical irreversibility *vs.* heterogeneity in the intrinsic chemical affinity.

Future work will investigate the utility of SSCP for identifying whether volume exclusion of the NP body from the operational reaction layer is in effect. As detailed herein, the available theoretical framework can account for this phenomenon in deriving metal speciation parameters from the experimental data. In the case of chemically heterogeneous complexants, the extent to which any such exclusion phenomena are manifest may vary along the SSCP wave depending on the interplay between the many contributing factors [82,137,138]. It is envisaged that strategic manipulation of measurement conditions and solution parameters will yield insights into volume exclusion of NP complexants from the operational reaction layer. For metal-humic systems, the demonstrated agreement between the degree of heterogeneity obtained from the shape of a single SSCP wave and that obtained from the slope of a double logarithmic $\overline{K}_{\mathrm{int}}$ *vs.* θ_{M} plot [145-147] confirms that any such effects do not impact on the observed chemical heterogeneity of the complexant under the solution and electrodic conditions studied to date. Rigorous description of kinetically controlled SSCP waves for chemically heterogeneous nanoparticulate metal complexes will require use of numerical methods to account for the coupled distance-dependent variation of the contributing thermodynamic and kinetic parameters.

Symbols and abbreviations

Latin

A_{el}	electrode surface area (m^2)
$c^{*}_{\mathrm{L,t}}$	total concentration of the reactive form of a molecular ligand L in bulk solution (mol m^{-3})
c^{*}_{M}	concentration of free metal ion in the bulk aqueous solution (mol m^{-3})
c_{M}	intraparticulate concentration of free metal ion (mol m^{-3})
$c^{*}_{\mathrm{M,t}}$	concentration of all metal species in the bulk aqueous solution (mol m^{-3})
$\bar{c}_{\mathrm{M^0}}$	mean concentration of reduced M in the electrode volume (mol m^{-3})
$c^{0}_{\mathrm{M^0}}$	concentration of reduced M at the electrode surface (mol m^{-3})
$\bar{c}^{\lambda}_{\mathrm{S}}$	average concentration of nanoparticulate reactive sites in the operational reaction layer zone at a macroscopic interface (mol m^{-3})
$c_{\mathrm{S,t}}$	total intraparticulate concentration of reactive sites (mol m^{-3})
$\bar{c}_{\mathrm{S,t}}$	smeared-out total concentration of reactive sites (mol m^{-3})
$\bar{c}_{\mathrm{M}}$	smeared-out concentration of intraparticulate free metal ion
c_{MS}	intraparticulate concentration of inner-sphere complexes (mol m^{-3})
$\bar{c}_{\mathrm{MS}}$	smeared-out concentration of inner-sphere complexes with nanoparticulate reactive sites (mol m^{-3})
$\bar{c}^{\lambda}_{\mathrm{MS}}$	average concentration of inner-sphere complexes with nanoparticulate reactive sites in the operational reaction layer zone at a macroscopic interface (mol m^{-3})

627	$\bar{D}$	weighted average diffusion coefficient of free M and its complexed forms in aqueous solution (m^2
628		s^{-1})
629	D_M	diffusion coefficient of free M in aqueous solution (m^2 s^{-1})
630	D_{ML}	diffusion coefficient of ML in aqueous solution (m^2 s^{-1})
631	D_p	diffusion coefficient of an NP in aqueous solution (m^2 s^{-1})
632	E_d	deposition potential (V)
633	DGT	diffusive gradients in thin film
634	DMT	Donnan membrane technique
635	$E_{d,1/2}$	half-wave deposition potential (V)
636	E_0^{eq}	equibrium potential at the end of the deposition step (V)
637	E_p	stripping peak potential (V)
638	$\bar{f}_B$	Boltzmann equilibrium partitioning factor
639	$\bar{f}_{el,a}$	electrostatic coefficient for conductive diffusion towards the NP
640	$\bar{f}_{el,d}$	electrostatic coefficient for conductive diffusion away from the NP
641	I_d^*	limiting value of the deposition current (A)
642	I_s	stripping current (A)
643	J_{dif}^*	diffusion controlled flux from bulk medium to macroscopic surface (mol m^{-2} s^{-1})
644	J_{kin}	kinetically controlled flux for dissociation of inner-sphere metal complexes within the reaction
645		layer (mol m^{-2} s^{-1})
646	$\bar{K}_{app}$	mean apparent stability constant of M-NP association (m^3 mol^{-1})
647	K_{int}	intrinsic stability contant of the inner-sphere complex MS (m^3 mol^{-1})
648	$\bar{K}_{int}$	mean intrinsic stability contant of all inner-sphere complexes MS (m^3 mol^{-1})
649	K^{os}	stability constant of an outer-sphere reactant pair (m^3 mol^{-1})
650	KK	Koutecký-Koryta
651	k_a	association rate constant (m^3 mol^{-1} s^{-1})
652	$k_{a,p}$	rate constant for diffusive supply of free M to an NP (m^3 mol^{-1} s^{-1})
653	k_a^{is}	rate constant for inner-sphere complex formation from the precursor outer-sphere complex in an NP
654		(m^3 mol^{-1} s^{-1})
655	k_d	dissociation rate constant (s^{-1})
656	$k_{d,p}$	rate constant for diffusion of M_{aq}^{z+} away from an NP (s^{-1})
657	k_d^{is}	rate constant for inner-sphere complex dissociation in an NP (s^{-1})
658	k_w	inner-sphere dehydration rate constant of hydrated metal ions (s^{-1})
659	L	molecular ligand
660	$\mathcal{L}$	lability parameter

661	$\mathcal{L}_{NP}$	lability parameter for nanoparticulate MS
662	M	free hydrated metal ion, M_{aq}^{z+}
663	MS	inner-sphere complex between M and S
664	NP	nanoparticle
665	NTA	nitrilotriacetic acid
666	PDCA	pyridine-2,6-dicarboxylic acid
667	PLM	permeation liquid membrane
668	$R_{a,p}$	rate of diffusive supply of $M_{aq}^{z_M^+}$ towards an NP (mol m^{-3} s^{-1})
669	R_a^{is}	rate of inner-sphere complex formation in an NP (mol m^{-3} s^{-1})
670	$R_{d,p}$	rate of diffusive efflux of $M_{aq}^{z_M^+}$ away from an NP (mol m^{-3} s^{-1})
671	R_d^{is}	rate of inner-sphere complex dissociation in an NP (mol m^{-3} s^{-1})
672	r_0	electrode radius (m)
673	r_p	nanoparticle radius (m)
674	S	reactive site on/within an NP
675	SCP	stripping chronopotentiometry
676	SSCP	scanned deposition potential stripping chronopotentiometry
677	t_d	deposition time (s)
678	$w_{1/2}$	width of an individual stripping peak at half the peak height (V)
679	V_{el}	electrode volume (m^3)
680		
681	Greek	
682	Γ	heterogeneity parameter
683	δ_M	diffusion layer thickness for the free metal ion (m)
684	$\overline{\delta}$	mean diffusion layer thickness for the metal complex system (m)
685	θ_M	ratio of concentrations of inner-sphere complexes and reactive sites
686	κ^{-1}	Debye screening length in bulk aqueous solution (m)
687	κ_p^{-1}	intraparticulate Debye screening length (m)
688	λ	reaction layer thickness (m)
689	$\overline{\lambda}$	thickness of the operational reaction layer at the macroscopic interface in the presence of
690		nanoparticulate metal complexes (m)
691	λ_{NP}	thickness of the intraparticulate reaction layer for a soft nanoparticle (m)
692	μ	dissociation reaction layer thickness (m)
693	τ	SCP transition (reoxidation) time (s)
694	τ^*	limiting value of the SCP transition (reoxidation) time (s)
695	τ_d	characteristic time constant of the deposition process (s)

Acknowledgements

RMT conducted this work within the framework of the EnviroStress Center of Excellence at Universiteit Antwerpen.

References

[1] J. Buffle, Complexation Reactions in Aquatic Systems. An Analytical Approach, Ellis Horwood, Chichester, 1988.

[2] H.P. van Leeuwen, J. Buffle, Voltammetry of heterogeneous metal complex systems. Theoretical analysis of the effects of association/dissociation kinetics and the ensuing lability criteria, J. Electroanal. Chem. 296 (1990) 359-370.

[3] D.R. Turner, M. Whitfield, The reversible electrodeposition of trace metal ions from multi-ligand systems. Part I. Theory, J. Electroanal. Chem. 103 (1979) 43-60.

[4] D.R. Turner, M. Whitfield, The reversible electrodeposition of trace metal ions from multi-ligand systems. Part II. Calculations on the electrochemical availability of lead at trace levels in seawater, J. Electroanal. Chem. 103 (1979) 61-79.

[5] R.M. Town, H. Emons, J. Buffle, Speciation analysis by electrochemical methods, in: R. Cornelis, H. Crews, J. Caruso, H. Heumann (Eds.), Handbook of Elemental Speciation: Techniques and Methodology, Wiley, New York, 2003, pp. 428-461.

[6] J. Buffle, M.L. Tercier, *In situ* voltammetry: concepts and practice for trace analysis and speciation, in: J. Buffle, G. Horvai (Eds), In Situ Monitoring of Aquatic Systems: Chemical Analysis and Speciation, John Wiley & Sons, Chichester, 2000, pp. 279-405.

[7] A.M. Mota, M.M. Correia dos Santos, Trace metal speciation of labile chemical species in natural waters: electrochemical methods, in: A. Tessier, D.R. Turner (Eds), Metal Speciation and Bioavailability in Aquatic Systems, John Wiley & Sons, Chichester, 1995, pp. 205-257.

[8] J. Buffle, M.-L. Tercier-Waeber, Voltammetric environmental trace-metal analysis and speciation: from laboratory to *in situ* measurements, Trends Anal. Chem. 24 (2005) 172-191.

[9] A.M. Mota, J.P. Pinheiro, M.L. Simões Gonçalves, Electrochemical methods for speciation of trace elements in marine waters. Dynamic aspects, J. Phys. Chem. A 116 (2012) 6433-6442.

[10] E. Companys, J. Galceran, J.P. Pinheiro, J. Puy, P. Salaun, A review on electrochemical methods for trace metal speciation in environmental media, Curr. Opin. Electrochem. 3 (2017) 144-162.

[11] N. Serrano, J.M. Díaz-Cruz, C. Ariño, M. Esteban, Stripping chronopotentiometry in environmental analysis, Electroanalysis 19 (2007) 2039-2049.

[12] D. Omanović, C. Garnier, K. Gibbon-Walsh, I. Pižeta, Electroanalysis in environmental monitoring: tracking trace metals – a mini review, Electrochem. Comm. 61 (2015) 78-83.

[13] J. Barton, M.B.G. Garcia, D.H. Santos, P. Fanjul-Bolado, A. Ribotti, M. McCaul, D. Diamond, P. Magni, Screen-printed electrodes for environmental monitoring of heavy metals ions: a review, Microchim. Acta 183 (2016) 503-517.

[14] J. Holmes, P. Pathirathna, P. Hashemi, Novel frontiers in voltammetric trace metal analysis: towards real time, on-site *in situ* measurements, Trends Anal. Chem. 111 (2019) 206-2019.

[15] G.M.S. Alves, L.S. Rocha, H.M.V.M. Soares, Multi-element determination of metals and metalloids in waters and wastewaters, at trace concentration level, using electroanalytical stripping methods with environmentally friendly mercury free-electrodes: a review, Talanta 175 (2017) 53-68.

[16] M. Díaz-de-Alba, M.D. Galindo-Riaño, J.P. Pinheiro, Lead electrochemical speciation analysis in seawater media by using AGNES and SSCP techniques, Environ. Chem. 11 (2014) 137-149.

[17] D. Omanović, M. Lovrić, A simulation of an anion-induced adsorption of metal ions in pseudopolarography using a thin mercury film covered rotating disk electrode, Electroanalysis 16 (2004) 563-571.

[18] F.C. Anson, J.B. Flanagan, K. Takahashi, A. Yamada, Some virtues of differential pulse polarography in examining adsorbed reactants, J. Electroanal. Chem. 67 (1976) 253-259.

[19] J. Buffle, A. Cominoli, Voltammetric study of humic and fulvic substances. Part IV. Behaviour of fulvic substances at the mercury-water interface, J. Electroanal. Chem. 121 (1981) 273-299.

[20] H.P. van Leeuwen, Reactant adsorption in analytical pulse polarography: an outline in terms of the concentration profile, J. Electroanal. Chem. 133 (1982) 201-209.

[21] H.P. van Leeuwen, M. Sluyters-Rehbach, K. Holub, The influence of reactant adsorption on limiting currents in normal pulse polarography. The ranges of low and high concentrations, J. Electroanal. Chem. 135 (1982) 13-24.

[22] H.P. van Leeuwen, J. Buffle, M. Lovric, Reactant adsorption in analytical pulse voltammetry: methodology and recommendations, Pure Appl. Chem. 64 (1992) 1015-1028.

[23] R.M. Town, H.P. van Leeuwen, Effects of adsorption in stripping chronopotentiometric metal speciation analysis. , J. Electroanal. Chem. 523 (2002) 1-15.

[24] R.M. Town, H.P. van Leeuwen, Significance of wave form parameters in stripping chronopotentiometric metal speciation analysis, J. Electroanal. Chem. 535 (2002), 11-25.

[25] J. Buffle, Calculation of the surface concentration of the oxidized metal during the stripping step in the anodic stripping techniques and its influence on speciation measurements in natural waters, J. Electroanal. Chem. 125 (1981) 273-294.

[26] A.M. Almeida Mota, J. Buffle, S.P. Kounaves, M.L. Simoes Goncalves, The importance of concentration effects at the electrode surface in anodic stripping voltammetric measurements of complexation of metal ions at natural water concentrations, Anal. Chim. Acta 172 (1985) 13-30.

[27] H.P. van Leeuwen, R.M. Town, Elementary features of depletive stripping chronopotentiometry, J. Electroanal. Chem. 535 (2002), 1-9.

[28] R.M. Town, H.P. van Leeuwen, Depletive stripping chronopotentiometry: a major step forward in electrochemical stripping techniques for metal ion speciation analysis, Electroanalysis 16 (2004) 458-471.

[29] H.P. van Leeuwen, R.M. Town, Electrochemical metal speciation analysis of chemically heterogeneous samples: the outstanding features of stripping chronopotentiometry at scanned deposition potential, Environ. Sci. Technol. 37 (2003) 3945-3952.

[30] R.M. Town, H.P. van Leeuwen, Comparative evaluation of scanned stripping techniques: SSCP vs SSV, Croat. Chem. Acta 79 (2006) 15-25.

[31] W. Davison, H. Zhang, Progress in understanding the use of diffusive gradients in thin films (DGT) – back to basics, Environ. Chem. 9 (2012) 1-13.

[32] J. Galceran, J. Puy, Interpretation of diffusion gradients in thin films (DGT) measurements: a systematic approach, Environ. Chem. 12 (2015), 112-122.

[33] L. Weng, W.H. van Riemsdijk, E.J.M. Temminghoff, Kinetic aspects of Donnan membrane technique for measuring free trace cation concentration, Anal. Chem. 77 (2005), 2582-2861.

[34] L. Weng, W.H. van Riemsdijk, E.J.M. Temminghoff, Effects of lability of metal complex on free ion measurement using DMT, Environ. Sci. Technol. 44 (2010) 2529-2534.

[35] Z. Zhang, J. Buffle, H.P. van Leeuwen, Roles of dynamic metal speciation and membrane permeability in metal flux through lipophilic membranes: general theory and experimental validation with nonlabile complexes, Langmuir 23 (2007), 5216-5226.

[36] L. Tomaszewski, J. Buffle, J. Galceran, Theoretical and analytical characterization of a flow-through permeation liquid membrane with controlled flux for metal speciation measurements, Anal. Chem. 75 (2003) 893-900.

[37] P. Gunkel-Grillon, J. Buffle, Speciation of Cu(II) with a flow-through permeation liquid membrane: discrimination between free copper, labile and inert Cu(II) complexes, under natural water conditions, Analyst 133 (2008) 954-961.

[38] L. Weng, F.A. Vega, W.H. van Riemsdijk, Strategies in the application of the Donnan membrane technique, Environ. Chem. 8 (2011) 466-474.

[39] H.P. van Leeuwen, R.M. Town, J. Buffle, R.F.M.J. Cleven, W. Davison, J. Puy, W.H. van Riemsdijk, L. Sigg, Dynamic speciation analysis and bioavailability of metals in aquatic systems, Environ. Sci. Technol. 39 (2005) 8545-8556.

[40] H.P. van Leeuwen, J.P. Pinheiro, Lability criteria for metal complexes in micro-electrode voltammetry, J. Electroanal. Chem. 471 (1999) 55-61.

[41] J. Galceran, J. Puy, J. Salvador, J. Cecília, H.P. van Leeuwen, Voltammetric lability of metal complexes at spherical microelectrodes with various radii, J. Electroanal. Chem. 505 (2001) 85-94.

[42] M. Lovrić, S. Komorsky-Lovrić, Influence of electrode radius on apparent lability of complex of amalgam forming ions, Int. J. Electrochem. Sci. 9 (2014) 5549-5559.

[43] K.W. Warnken, W. Davison, H. Zhang, J. Galceran, J. Puy, In situ measurements of metal complex exchange kinetics in freshwater, Environ. Sci. Technol. 41 (2007) 3179-3185.

[44] K.W. Warnken, W. Davison, H. Zhang, Interpretation of in situ speciation measurements of inorganic and organically complexed trace metals in freshwater by DGT, Environ. Sci. Technol. 42 (2008), 6903-6909.

[45] T. Yapici, I.I. Fasfous, J. Murimboh, C.L. Chakrabarti, Investigation of DGT as a metal speciation technique for municipal wastes and aqueous mine effluents, Anal. Chim. Acta 622 (2008) 70-76.

[46] Z. Wu, M. He, C. Lin, In situ measurements of concentrations of Cd, Co, Fe and Mn in estuarine porewater using DGT, Environ. Poll. 159 (2011) 1123-1128.

[47] N.J. Lehto, W. Davison, H. Zhang, The use of ultra-thin diffusive gradients in thin-films (DGT) devices for the analysis of trace metal dynamic in soils and sediments: a measurement and modelling approach, Environ. Chem. 9 (2012) 415-423.

[48] M. Eigen, Fast elementary steps in chemical reaction mechanisms, Pure Appl. Chem. 6 (1963) 97-115.

[49] M. Eigen, R.G. Wilkins, The kinetics and mechanism of formation of metal complexes. Adv. Chem. Ser. 49 (1965) 55-80.

[50] F.M.M. Morel, J.G. Hering, Principles and Applications of Aquatic Chemistry, Wiley, New York, 1993.

[51] J. Heyrovský, J. Kůta, Chapter XVII in Principles of Polarography, Academic Press, New York, 1966.

[52] R. Brdička, K. Wiesner, Polarographic determination of the rate of the reaction between ferrohem and hydrogen peroxide, Collect. Czech. Chem. Commun. 12 (1947) 39-63.

[53] J. Koutecký, Theorie langsamer elektrodenreaktionen in der polarographie und polarographisches verhalten eines systems, bei welchem der depolarisator durch eine schnelle chemische reaction aus einem elektroinaktiven stoff entsteht, Collect. Czech. Chem. Commun. 18 (1953) 597-610.

[54] H.P. van Leeuwen, J. Puy, J. Galceran, J. Cecília, Evaluation of the Koutecký-Koryta approximation for voltammetric currents generated by metal complex systems with various labilities, J. Electroanal. Chem. 526 (2002) 10-18.

[55] H.G. de Jong, H.P. van Leeuwen, Voltammetry of metal complex systems with different diffusion coefficients of the species involved. Part I. Analytical approaches to the limiting current for the general case including association/dissociation kinetics, J. Electroanal. Chem. 234 (1987) 1-16.

[56] H.G. de Jong, H.P. van Leeuwen, Voltammetry of metal complex systems with different diffusion coefficients of the species involved. Part II. Behaviour of the limiting current and its dependence on association/dissociation kinetics and lability, J. Electroanal. Chem. 234 (1987) 17-29.

[57] H.G. de Jong, H.P. van Leeuwen, Voltammetry of metal complex systems with different diffusion coefficients of the species involved. Part III. The current-potential relation for the general case including association/dissociation kinetics, J. Electroanal. Chem. 235 (1987) 1-10.

[58] H.P. van Leeuwen H.G. de Jong, K. Holub, Voltammetry of metal complex systems with different diffusion coefficients of the species involved. Part IV. Simulation of the limiting current for any metal-to-ligand ratio and elaboration to voltammetric titration curves, J. Electroanal. Chem. 260 (1989) 213-220.

[59] D. Alemani, B. Chopard, J. Galceran, J. Buffle, LBGK method coupled to time splitting technique for solving reaction-diffusion processes in complex systems, Phys. Chem. Chem. Phys. 7 (2005) 3331-3341.

[60] E. Laborda, J.M. Olmos, F. Martínez-Ortiz, A. Molina, Voltammetric speciation studies of systems where the species diffusivities differ significantly, J. Solid State Electrochem. 19 (2015) 549-561.

[61] H.P. van Leeuwen, R.M. Town, J. Buffle, Impact of ligand protonation on Eigen-type metal complexation kinetics in aqueous systems, J. Phys. Chem. A 111 (2007) 2115-2121.

[62] R.M. Town, H.P. van Leeuwen, Impact of ligand protonation on higher-order metal complexation kinetics in aqueous systems, J. Phys. Chem. A 112 (2008) 2563-2571.

[63] H.P. van Leeuwen, R.M. Town, Protonation effects on dynamic flux properties of aqueous metal complexes, Collect. Czech. Chem. Commun. 74 (2009) 1543-1557.

[64] H.P. van Leeuwen, R.M. Town, Outer-sphere and inner-sphere ligand protonation in metal complexation kinetics: the lability of ETDA complexes, Environ. Sci. Technol. 43 (2009) 88-93.

[65] J. Puy, J. Cecília, J. Galceran, R.M. Town, H.P. van Leeuwen, Voltammetric lability of multiligand complexes: the case of ML_2, J. Electroanal. Chem. 571 (2004) 121-132.

[66] J. Salvador, J. Puy, J. Galceran, J. Cecília, R.M. Town, H.P. van Leeuwen, Lability criteria for successive metal complexes in steady-state planar diffusion, J. Phys. Chem. B 110 (2006) 891-899.

[67] J. Salvador, J.L. Garcés, J. Galceran, J. Puy, Lability of a mixture of metal complexes under steady-state planar diffusion in a finite domain, J. Phys. Chem. B 110 (2006) 13661-13669.

[68] J. Salvador, J.L. Garcés, E. Companys, J. Cecília, J. Galceran, J. Puy, R.M. Town, Ligand mixture effects in metal complex lability, J. Phys. Chem. A 111 (2007) 4304-4311.

[69] Z. Zhang, J. Buffle, R.M. Town, J. Puy, H.P. van Leeuwen, Metal flux in ligand mixtures. 2. Flux enhancement due to kinetic interplay: comparison of the reaction layer approximation with a rigorous approach, J. Phys. Chem. A 113 (2009) 6572-6580.

[70] J. Buffle, K. Startchev, J. Galceran, Computing steady-state metal flux at microorganism and bioanalogical sensor interfaces in multiligand systems. A reaction layer approximation and its comparison with the rigorous solution, Phys. Chem. Chem. Phys. 9 (2007) 2844-2855.

[71] Z. Zhang, J. Buffle, Interfacial metal flux in ligand mixtures. 3. Unexpected flux enhancement due to kinetic interplay at the consuming surface, computed for aquatic systems, Environ. Sci. Technol. 43 (2009) 5762-5768.

[72] W.-W. Yang, A.-J. Miao, L.-Y. Yang, Cd^{2+} toxicity to a green alga *Chlamydomonas reinhardtii* as influenced by its adsorption on TiO_2 engineered nanoparticles. PLoS ONE 7 (2012) e32300.

[73] W. Fan, T. Liu, X. Li, R. Peng, Y. Zhang, Nano-TiO_2 affects Cu speciation, extracellular enzyme activity, and bacterial communities in sediments, Environ. Poll. 218 (2016) 77-85.

[74] X. Tao, Y. He, J.D. Fortner, Y. Chen, J.B. Hughes, Effects of aqueous stable fullerene nanocrystal (nC_{60}) on copper (trace necessary nutrient metal): enhanced toxicity and accumulation of copper in *Daphnia magna*, Chemosphere 92 (2013) 1245-1252.

[75] X. Wang, R. Qu, J. Liu, Z. Wei, L. Wang, S. Yang, Q. Huang, Z. Wang, Effect of different carbon nanotubes on cadmium toxicity to *Daphnia magna*: the role of catalyst impurities and adsorption capacity, Environ. Poll. 208 (2016) 732-738.

[76] W.-W. Yang, Y. Wang, B. Huang, N.-X. Wang, Z.-B. Wei, J. Luo, A.-J. Miao, L.-Y. Yang, TiO_2 nanoparticles act as a carrier of Cd bioaccumulation in the ciliate *Tetrahymena thermophila*, Environ. Sci. Technol. 48 (2014) 7568-7575.

[77] H.P. van Leeuwen, J. Duval, J.P. Pinheiro, R. Blust, R.M. Town, Chemodynamics and bioavailability of metal ion complexes with nanoparticles in aqueous media, Environ. Sci.: Nano 4 (2017) 2108-2133.

[78] J.P. Pinheiro, M. Minor, H.P. van Leeuwen, Metal speciation dynamics in colloidal ligand dispersions, Langmuir 21 (2005) 8635-8642.

[79] H.P. van Leeuwen, Eigen kinetics in surface complexation of aqueous metal ions, Langmuir 24 (2008) 11718-11721.

[80] H.P. van Leeuwen, J. Buffle, J.F.L. Duval, R.M. Town, Understanding the extraordinary ionic reactivity of aqueous nanoparticles, Langmuir 29 (2013) 10297-10302

[81] R.M. Town, J. Buffle, J.F.L. Duval, H.P. van Leeuwen, 2013. Chemodynamics of soft charged nanoparticles in aquatic media: fundamental concepts, J. Phys. Chem. A 117 (2013) 7643-7654.

[82] J.F.L. Duval, Chemodynamics of metal ion complexation by charged nanoparticles: a dimensionless rationale for soft, core-shell and hard particle types, Phys. Chem. Chem. Phys. 19 (2017) 11802-11815.

[83] P.L.R. van der Veeken, J.P. Pinheiro, H.P. van Leeuwen, Metal speciation by DGT/DET in colloidal complex systems, Environ. Sci. Technol. 42 (2008) 8835-8840.

[84] P.L.R; van der Veeken, P. Chakraborty, H.P. van Leeuwen, Accumulation of humic acid in DET/DGT gels, Environ. Sci. Technol. 44 (2010) 4253-4257.

[85] P.L.R. van der Veeken, H.P. van Leeuwen, DGT/DET gel partition features of humic acid/metal species, Environ. Sci. Technol. 44 (2010) 5523-5527.

[86] P.L.R. van der Veeken, H.P. van Leeuwen, Gel-water partitioning of soil humics in diffusive gradient in thin film (DGT) analysis of their metal complexes, Environ. Chem. 9 (2012) 24-30.

[87] H.P. van Leeuwen, Steady-state DGT fluxes of nanoparticulate metal complexes, Environ. Chem. 8 (2011) 525-528.

[88] H.P. van Leeuwen, Revisited: DGT speciation analysis of metal-humic acid complexes, Environ. Chem. 13 (2016) 84-88.

[89] A.L.-T. Pham, C. Johnson, D. Manley, H. Hsu-Kim, Influence of sulfide nanoparticles on dissolved mercury and zinc quantification by diffusive gradient in thin-film passive samplers, Environ. Sci. Technol. 49 (2015) 12897-12903.

[90] R.M. Town, H.P. van Leeuwen, Fundamental features of metal ion determination by stripping chronopotentiometry, J. Electroanal. Chem. 509 (2001) 58-65. Corrigendum: J. Electroanal. Chem. 515 (2001) 129.

[91] H.P. van Leeuwen, R.M. Town, Stripping chronopotentiometry at scanned deposition potential (SSCP). Part 1. Fundamental features, J. Electroanal. Chem. 536 (2002) 129-140.

[92] C. Parat, A. Schneider, A. Castetbon, M. Potin-Gautier, Determination of trace metal speciation parameters by usng screen-printed electrodes in stripping chronopotentiometry without deaerating, Anal. Chim. Acta 688 (2011) 156-162.

[93] R.M. Town, H.P. van Leeuwen, Stripping chronopotentiometry at scanned deposition potential (SSCP). Part 5. Features of multi-metal systems, J. Electroanal. Chem. 573 (2004) 147-157.

[94] H.P. van Leeuwen, R.M. Town, Stripping chronopotentiometry at scanned deposition potential (SSCP). Part 3. Irreversible electrode reaction, J. Electroanal Chem. 556 (2003) 93-102.

[95] J.G. Lawson, D.A. Aikens, Mechanism and thermodynamics of the polarographic deposition of aquo In(III), J. Electroanal. Chem. Interf. Electrochem. 15 (1967) 193-209.

[96] J.P. Pinheiro, L.S. Rocha, D. Goveia, R.M. Town, Scanned stripping chronopotentiomety at bismuth film rotating disc electrodes: a method for quantitative dynamic metal speciation, Environ. Chem. 11 (2014) 150-157.

[97] H.P. van Leeuwen, R.M. Town, Adsorptive stripping chronopotentiomery (AdSCP). Part 1: Fundamental features, J. Electroanal. Chem. 610 (2007) 9-16.

[98] R.M. Town, H.P. van Leeuwen, Adsorptive stripping chronopotentiomery (AdSCP). Part 2: Basic experimental features, J. Electroanal. Chem. 610 (2007) 17-27.

[99] R.M. Town, H.P. van Leeuwen, Stripping chronopotentiometry at scanned deposition potential (SSCP). Part 2. Determination of metal ion speciation parameters, J. Electroanal Chem. 541 (2003) 51-65.

[100] S. Noel, J. Buffle, N. Fatin-Rouge, J. Labille, Factors affecting the flux of macromolecular, labile, metal complexes at consuming interfaces, in water and inside agarose gel: SSCP study and environmental implications, J. Electroanal. Chem. 595 (2006) 125-135.

[101] L.S. Rocha, W.G. Botero, N.G. Alves, J.A. Moreira, A.M.R. da Costa, J.P. Pinheiro, Ligand size polydispersity effect on SSCP signal interpretation, Electrochim. Acta 166 (2015) 395-402.

[102] J.P. Pinheiro, R. Domingos, R. Lopez, R. Brayner, F. Fiévet, K. Wilkinson, Determination of diffusion coefficients of nanoparticles and humic substances using scanning stripping chronopotentiometry (SSCP), Coll. Surf. A: Physicochem. Eng. Aspects 295 (2007) 200-208.

[103] W. Davison, Defining the electroanalytically measured species in a natural water sample, J. Electroanal. Chem. 87 (1978) 395-404.

[104] H.P. van Leeuwen, Revisited: the conception of lability of metal complexes, Electroanalysis 13 (2001) 826-830.

[105] G. Anderegg, Pyridinederivate als Komplexbildner I. Pyridincarbonsäuren, Helv. Chim. Acta 43 (1960) 414-424?

[106] M. von Stackelberg, M. Pilgram, V. Toome, Bestimmung von Diffusionskoeffizienten einiger Ionen in wäβriger Lösung in Gegenwart von Fremdelektrolyten. I, Z. Elektrochem. 57 (1953) 342-350.

[107] R.M. Town, J.P. Pinheiro, R. Domingos, H.P. van Leeuwen, Stripping chronopotentiometry at scanned deposition potential (SSCP). Part 6: Features of irreversible systems, J. Electroanal Chem. 580 (2005) 57-67.

[108] H.P. van Leeuwen, R.M. Town, Stripping chronopotentiometry at scanned deposition potential (SSCP). Part 4. The kinetic current regime, J. Electroanal Chem. 561 (2004) 67-74.

[109] H.P. van Leeuwen, R.M. Town, Stripping chronopotentiometry at scanned deposition potential (SSCP). Part 7. Kinetic currents for ML_2 complexes, J. Electroanal Chem. 587 (2006) 148-154.

[110] E. Rotureau, Y. Waldvogel, R.M. Présent, J.P. Pinheiro, Addressing temperature effects on metal chemodynamics studies using stripping electroanalytical techniques. Part 1: Lability of small complexes, J. Electroanal. Chem. 752 (2015) 68-74.

[111] N. Serrano, J.M. Díaz-Cruz, C. Ariño, M. Esteban, J. Puy, E. Companys, J. Galceran, J. Cecília, Full-wave analysis of stripping chronopotentiograms at scanned deposition potential (SSCP) as a tool for heavy metal speciation: theoretical development and application to Cd(II) phthalate and Cd(II)-iodide systems. J. Electroanal. Chem. 600 (2007) 275-284.

[112] R.M. Town, H.P. van Leeuwen, Dynamic speciation analysis of heterogeneous metal complexes with natural ligands by stripping chronopotentiometry at scanned deposition potential (SSCP), Aust. J. Chem. 57 (2004) 983-992.

[113] E. Rotureau, Analysis of metal speciation dynamics in clay minerals dispersion by stripping chronopotentiometry techniues, Coll. Surf. A: Physicochem. Eng. Aspects 441 (2014) 291-297. https://doi.org/10.1016/j.colsurfa.2013.09.006

[114] V.G. Levich, Physicochemical Hydrodynamics, Prentice Hall, Englewood Cliffs, NJ, 1962, Chapter 2, pp. 39-138.

[115] J.M. Díaz-Cruz, C. Ariño, M. Esteban, E. Casassas, Polarography and anodic stripping voltammetry of metal-polycarboxylate complexes: phenomenological relationship between limiting currents and hydrodynamic mass transport, J. Electroanal. Chem. 333 (1992) 33-45.

[116] J.C. Ball, R.G. Compton, Anodic stripping voltammetry at hydrodynamic mercury thin film electrodes. Numerical simulation of stripping peaks for reversible processes at uniformly accessible electrodes, Electroanalysis 9 (1997) 765-769.

[117] M. Esteban, H.G. De Jong, H.P. van Leeuwen, Metal speciation in polyelectrolytic systems by differential pulse anodic stripping voltammetry, Intern. J. Environ. Anal. Chem. 38 (1990) 75-83.

[118] J. Koutecký, J. Koryta, The general theory of polarographic kinetic currents, Electrochim. Acta 3 (1961) 318-339.

[119] J. Koryta, J. Dvorak, L. Kavan, Principles of Electrochemistry, 2nd edn. Wiley, Chichester, 1993.

[120] R.M. Fuoss, Ionic association. III. The equilibrium between ion pairs and free ions, J. Am. Chem. Soc. 80 (1958) 5059-5061.

[121] J.P. Pinheiro, H.P. van Leeuwen, Scanned stripping chronopotentiometry of metal complexes: lability diagnosis and stability computation, J. Electroanal. Chem. 570 (2004) 69-75.

[122] J. Koryta, Kinetik der Elektrodenvorgänge von Komplexen in der Polarographie III. Durchtritts- und Dissoziationsreaktion des Komplexes, Coll. Czech. Chem. Commun. 24 (1959) 3057-3074.

[123] M.S. Shuman, I. Shain, Study of the chemical reaction preceding reduction of cadmium nitriloacetic acid complexes using stationary electrode polarography, Anal. Chem. 41 (1969) 1818-1825.

[124] K.R. Bullock, D.E. Smith, Fundamental and second harmonic alternating current polarography of electrode processes with coupled first-order preceding chemical reactions: experimental study of the cadmium-nitrilotriacetate system. Anal. Chem. 46 (1974) 1069-1074.

[125] G. Anderegg, S. Malik, Komplexone XLVII. The stability of palladium(II) complexes with aminopolycarboxylate anions, Helv. Chim. Acta 59 (1976) 1498-1511.

[126] G. Schwarzenbach, R. Gut, Die Komplexe der Seltenen Erdkationen und die Gadoliniumecke, Helv. Chim. Acta 39 (1956) 1589-1599.

[127] J. Crank, The Mathematics of Diffusion, Oxford Science Publications, Oxford, 1979.

[128] H. Ohshima, Electrophoresis of soft particles. Adv. Colloid Interf. Sci. 62 (1995) 189-235.

[129] J.F.L. Duval, Electrokinetics of soft interfaces. 2. Analysis based on the nonlinear Poisson-Boltzmann equation, Langmuir 21 (2005) 3247-3258.

[130] R.M. Town, J.F.L. Duval, J. Buffle, H.P. van Leeuwen, Chemodynamics of metal complexation by natural soft colloids: Cu(II) binding by humic acid. J. Phys. Chem. A 116 (2012) 6489-6496.

[131] H.P. van Leeuwen, J. Buffle, R.M. Town, Electric relaxation processes in chemodynamics of aqueous metal complexes: from simple ligands to soft nanoparticulate complexants, Langmuir 28 (2012) 227-234.

[132] J.F.L. Duval, H.P. van Leeuwen, Rates of ionic reactions with charged nanoparticles in aqueous media, J. Phys. Chem. A 116 (2012) 6443-6451.

[133] R.M. Town, H.P. van Leeuwen, R. Blust, Biochemodynamic features of metal ions bound by micro- and nano-plastics in aquatic media, Front. Chem. 6 (2018) 627.

[134] R.M. Town, H.P. van Leeuwen, Intraparticulate speciation analysis of soft nanoparticulate metal complexes. The impact of electric condensation on the binding of Cd^{2+}/Pb^{2+}/Cu^{2+} by humic acids, Phys. Chem. Chem. Phys. 18 (2016) 10049-10058.

[135] R.M. Town, J.P. Pinheiro, H.P. van Leeuwen, Chemodynamics of soft nanoparticulate metal complexes: from the local particle/medium interface to a macroscopic sensor surface, Langmuir 33 (2017) 527-536.

[136] H.P. van Leeuwen, R.M. Town, Lability of nanoparticulate metal complexes in electrochemical speciation analysis, J. Solid State Electrochem., 20 (2016) 3255-3262.

[137] J.F.L. Duval, R.M. Town, H.P. van Leeuwen, Applicability of the reaction layer principle to nanoparticulate metal complexes at a macroscopic reactive (bio)interface: a theoretical study, J. Phys. Chem. C 121 (2017) 19147-19161.

[138] J.F.L. Duval, R.M. Town, H.P. van Leeuwen, Lability of nanoparticulate metal complexes at a macroscopic metal responsive (bio)interface: expression and asymptotic scaling laws, J. Phys. Chem. C 122 (2018) 6052-6065.

[139] J.H.A.M. Wonders, Electrochemical Metal Speciation in Colloidal Dispersions, PhD thesis, Wageningen University, The Netherlands, 1995.

[140] J.H.A.M. Wonders, H.P. van Leeuwen, Voltammetric metal titration of particle dispersions, J. Electroanal. Chem. 401 (1996) 103-112.

[141] J.F.L. Duval, K.J. Wilkinson, H.P. van Leeuwen, J. Buffle, Humic substances are soft and permeable: evidence from their electrophoretic mobilities, Environ. Sci. Technol. 39 (2005) 6435-6445.

[142] J. Buffle, J.J. Vuilleumier, M.L. Tercier, N. Parthasarathy, Voltammetric study of humic and fulvic substances V. Interpretation of metal ion complexation measured by anodic stripping voltammetric methods, Sci. Total Environ. 60 (1987) 75-96.

[143] F. Berbel, J.M. Díaz-Cruz, C. Ariño, M. Esteban, F. Mas, J.L. Garcés, J. Puy, Voltammetric analysis of heterogeneity in metal ion binding by humics, Environ. Sci. Technol. 35 (2001) 1097-1102.

[144] M. Torrent, J. Puy, E. Companys, J. Galceran, J. Salvador, J.L. Garcés, F. Mas, Voltammetry of heterogeneous labile metal-macromolecular systems for any ligand to metal ratio: part IV. Binding curve from the polarographic waves, J. Electroanal. Chem. 577 (2005) 311-321.

[145] R.M. Town, H.P. van Leeuwen, Intraparticulate metal speciation analysis of soft complexing nanoparticles. The intrinsic chemical heterogeneity of metal-humic acid complexes, J. Phys. Chem. A 120 (2016) 8637-8644.

[146] R.M. Town, J.F.L. Duval, H.P. van Leeuwen, The intrinsic stability of metal ion complexes with nanoparticulate fulvic acids, Environ. Sci. Technol. 52 (2018) 11682-11690.

[147] R.M. Town, H.P. van Leeuwen, J.F.L. Duval, Rigorous physicochemical framework for metal ion binding by aqueous nanoparticulate humic subtances: implications for speciation modeling by the NICA-Donnan and WHAM codes, Environ. Sci. Technol. (2019), 53 (2019) 8516-8532.